Author(s): Vuornos, Kaisa; Ojansivu, Miina; Koivisto, Janne T.; Häkkänen, Heikki; Belay, Birhanu; Montonen, Toni; Huhtala, Heini; Kääriäinen, Minna; Hupa, Leena; Kellomäki, Minna; Hyttinen, Jari; Ihalainen, Janne; Miettinen, Susanna

Title: Bioactive glass ions induce efficient osteogenic differentiation of human adipose stem cells encapsulated in gellan gum and collagen type I hydrogels

Year: 2019

Version: Accepted version (Final draft)

Please cite the original version:

Vuornos, K., Ojansivu, M., Koivisto, J. T., Häkkänen, H., Belay, B., Montonen, T., Huhtala, H., Kääriäinen, M., Hupa, L., Kellomäki, M., Hyttinen, J., Ihalainen, J., & Miettinen, S. (2019). Bioactive glass ions induce efficient osteogenic differentiation of human adipose stem cells encapsulated in gellan gum and collagen type I hydrogels. Materials Science and Engineering C, 99, 905-918. https://doi.org/10.1016/j.msec.2019.02.035

Bioactive glass ions induce efficient osteogenic differentiation of human adipose stem cells encapsulated in gellan gum and collagen type I hydrogels

Kaisa Vuornos[a,b,*], Miina Ojansivu[a,b], Janne T Koivisto[c,d], Heikki Häkkänen[e], Birhanu Belay[f], Toni Montonen[f], Heini Huhtala[g], Minna Kääriäinen[h], Leena Hupa[i], Minna Kellomäki[c], Jari Hyttinen[f], Janne A Ihalainen[e], Susanna Miettinen[a,b]

[a]*Adult Stem Cell Group, BioMediTech, Faculty of Medicine and Health Technology , Tampere University, Tampere, Finland. P.O. BOX 100, FI-33014 Tampere University, Finland,*

kaisa.vuornos@tuni.fi, miina.ojansivu@ki.se, susanna.miettinen@tuni.fi.

[b]*Research, Development and Innovation Centre, Tampere University Hospital, Tampere, Finland. P.O. BOX 2000, FI-33521 Tampere, Finland.*

[c]*Biomaterials and Tissue Engineering Group, BioMediTech, Faculty of Medicine and Health Technology , Tampere University, Tampere, Finland. P.O. BOX 527, FI-33101 Tampere, Finland,*janne.t.koivisto@tuni.fi, minna.kellomaki@tuni.fi.

[d]*Heart Group, BioMediTech, Faculty of Medicine and Health Technology , Tampere University, Tampere, Finland. P.O. BOX 100, FI-33014 Tampere University, Finland.*

[e]*Nanoscience Center, University of Jyväskylä, Jyväskylä, Finland. P.O. BOX 35, FI-40014 University of Jyväskylä, Finland,* heikki.hakkanen@jyu.fi, janne.ihalainen@jyu.fi.

[f]*Computational Biophysics and Imaging Group, BioMediTech, Faculty of Medicine and Health Technology , Tampere University, Tampere, Finland. P.O. BOX 527, FI-33101 Tampere, Finland,* birhanu.belay@tuni.fi, toni.montonen@tuni.fi, jari.hyttinen@tuni.fi.

[g]*Faculty of Social Sciences, Tampere University, Tampere, Finland. P.O. BOX 100, FI-33014 Tampere University, Finland,* heini.huhtala@tuni.fi.

[h]*Department of Plastic and Reconstructive Surgery, Tampere University Hospital, P.O. BOX 2000, FI-33521 Tampere, Finland,* minna.kaariainen@pshp.fi

[i]*Johan Gadolin Process Chemistry Centre, Åbo Akademi University, Åbo, Finland. Biskopsgatan 8, FI-20500 Åbo, Finland,* leena.hupa@abo.fi.

*Corresponding author. Address: Tampere University, BioMediTech, Faculty of Medicine and Health Technology, Adult Stem Cell Group, P.O. BOX 100, FI-33014 Tampere University, Finland; Tel.: +358 40 190 1789; Fax: +358 3 3551 8498; E-mail: kaisa.vuornos@tuni.fi (K. Vuornos).

Abstract

Background: Due to unmet need for bone augmentation, our aim was to promote osteogenic differentiation of human adipose stem cells (hASCs) encapsulated in gellan gum (GG) or collagen type I (COL) hydrogels with bioactive glass (experimental glass 2-06 of composition [wt-%]: Na_2O 12.1, K_2O 14.0, CaO 19.8, P_2O_5 2.5, B_2O_3 1.6, SiO_2 50.0) extract based osteogenic medium (BaG OM) for bone construct development. GG hydrogels were crosslinked with spermidine (GG-SPD) or BaG extract (GG-BaG).

Methods: Mechanical properties of cell-free GG-SPD, GG-BaG, and COL hydrogels were tested in osteogenic medium (OM) or BaG OM at 0, 14, and 21d. Hydrogel embedded hASCs were cultured in OM or BaG OM for 3, 14, and 21d, and analyzed for viability, cell number, osteogenic gene expression, osteocalcin production, and mineralization. Hydroxyapatite-stained GG-SPD samples were imaged with Optical Projection Tomography (OPT) and Selective Plane Illumination Microscopy (SPIM) in OM and BaG OM at 21d. Furthermore, Raman spectroscopy was used to study the calcium phosphate (CaP) content of hASC-secreted ECM in GG-SPD, GG-BaG, and COL at 21d in BaG OM.

Results: The results showed viable rounded cells in GG whereas hASCs were elongated in COL. Importantly, BaG OM induced significantly higher cell number and higher osteogenic gene expression in COL. In both hydrogels, BaG OM induced strong mineralization confirmed as CaP by Raman spectroscopy and significantly improved mechanical properties. GG-BaG hydrogels rescued hASC mineralization in OM. OPT and SPIM showed homogeneous 3D cell distribution with strong mineralization in BaG OM. Also, strong osteocalcin production was visible in COL.

Conclusions: Overall, we showed efficacious osteogenesis of hASCs in 3D hydrogels with BaG OM with potential for bone-like grafts.

Keywords: adipose stem cell, bioactive glass, osteogenic differentiation, gellan gum hydrogel, collagen type I hydrogel

1. Introduction

Increasing number of musculoskeletal defects and the growth of the ageing population augment the demand for functional engineered bone grafts. Autologous bone is limited while, besides shortage of allograft bone, it might also pose a risk of adverse effects and graft rejection [1, 2]. Human adipose stem cells (hASCs) are abundant and accessible adult stem cells and suitable for the development of bone constructs [3]. For bone applications, 3D hydrogels offer an adaptable approach of a free form construct with high elasticity and malleable mechanical properties, instead of limited conventional scaffold structure. 3D hydrogel culture simulates more effectively the natural elastic cell microenvironment allowing higher degrees of freedom to form cellular interactions compared to traditional stiffer biomaterials. For instance, natural polymers have been studied as native microenvironments for stem cells, such as protein based collagen type I (COL), while inexpensive polysaccharide gellan gum (GG) offers more tailorable mechanical properties to support stem cell differentiation. Moreover, GG and COL hydrogels have been already reported as hydrophilic, biocompatible, bioresorbable, and also, adaptable hydrogel scaffolds suitable for bone tissue engineering applications [4-9]. On the other hand, bioactive glasses (BaGs) have been widely applied as medical implant materials and have been shown well applicable for bone grafts [10-12] and, in addition, as strong osteogenic inducers of the hASCs without any added chemical supplements such as growth factors [13, 14].

Despite their suitability for bone applications, hydrogel biomaterials in themselves lack bone mineralization enhancing components. To date, the majority of the GG and COL hydrogel studies for bone applications have sought to increase hydrogel mineralization and mechanical properties by the addition of nanosized or larger BaG particles to the hydrogel matrix [4, 7, 15, 16]. Hydrogel mineralization requires robust support from added components in *in vitro* conditions mimicking the

physiological conditions. To achieve this, in an earlier study, we demonstrated that BaG dissolution ions were strong inducers of hASC osteogenic differentiation, and showed that the ions dissolved from the specific composition of experimental silica-based BaG 2-06 combined with osteogenic medium (OM) components induced calcium phosphate (CaP) mineral accumulation already after 14 days of culture in 2D culture conditions [13]. The ionic dissolution products of experimental glass 2-06 have been previously analyzed high in Ca^{2+}, K^{+}, and B^{+}, and the detailed ionic composition of the bioactive glass extract (BaG ext) of experimental glass 2-06 has been reported in a published study [13]. Thus, we hypothesized that the BaG ext ionic dissolution products would promote equally strong osteogenic differentiation of hASCs in 3D hydrogel culture. In addition, since small molecules like cationic spermidine (SPD) have been demonstrated to interact with anionic polymers such as GG [17, 18], we hypothesized the divalent Ca^{2+} cations in the BaG ext to function as potential ionic crosslinkers for GG hydrogel. To the best of our knowledge, GG and COL have not been previously combined with BaG ionic species alone for bone tissue engineering applications with embedded hASCs. We also used efficient imaging techniques to assess the cell distribution, form and mineralization with in-house-built Optical Projection Tomography (OPT) and Selective Plane Illumination Microscopy (SPIM) systems that have been already applied to cell imaging in 3D hydrogel culture, mass transport studies, and characterization of 3D hydrogels [19-21].

Therefore, the aim of this study was to develop an effective hASC-laden hydrogel mineralization method for the development of engineered bone constructs. The mechanical properties of cell-free hydrogels were tested for bone applications with or without incubation in serum-containing OM and BaG ext based osteogenic medium (BaG OM) media. GG and COL hydrogels combined with BaG OM induction were compared for osteogenic differentiation of hydrogel-encapsulated hASCs, and to that end hASC viability, adhesion, cell number, osteocalcin production by immunofluorescence staining, mineralization, and the gene expression of osteogenic marker genes were analyzed. Additionally, the potential of GG ionic crosslinkers SPD and BaG ext to support hASC

mineralization was tested in the control OM. The transparent GG-SPD cell-hydrogel sample mineralized residues were imaged with OPT and SPIM in OM and BaG OM at 3 weeks. Also, the Raman spectra of hASC-secreted ECM and mineralized residues in GG-SPD, GG-BaG, and COL was measured at 3 weeks of culture in the BaG OM condition.

2. Materials and methods

2.1 Hydrogel scaffolds

2.1.1 Gellan gum hydrogel scaffolds. GG (low acyl, M_w 1.0 kg/mol; Gelzan CM; Sigma-Aldrich, St. Louis, MO, USA) sterile filtered (0.2 µm) solution of 0.5 % (w/v) concentration was crosslinked with either 16 % (v/v) SPD (BioXtra; Sigma-Aldrich) of 1 mg/mL concentration in 10 % (w/w) sucrose (Sigma-Aldrich) in deionized water or with BaG ext (experimental glass 2-06) [13] containing Dulbecco's Modified Eagle Medium/Ham's Nutrient Mixture F-12 (DMEM/F-12 1:1; Thermo Fisher Scientific, Waltham, MA, USA), 1 % L-glutamine (GlutaMAX; Thermo Fisher Scientific), and 1 % antibiotics/antimycotic containing 100 U/mL penicillin/100 U/mL streptomycin (P/S; Lonza, Basel, Switzerland) to yield GG-BaG hydrogel samples. The cell pellet was resuspended into GG solution at +37°C for hASC encapsulation into 3D hydrogel. The cell-hydrogel solution was manually mixed to an ionic crosslinker for immediate gelation. The cell culture medium was added on top of the gelated hASC-laden hydrogel samples.

2.1.2 Collagen type I hydrogel scaffolds. Commercially available COL (rat tail collagen type I, 3.0 mg/mL, Gibco; Thermo Fisher Scientific) was gelated with 10x phosphate buffered saline (10x PBS; Lonza) and 1 N NaOH (Sigma-Aldrich) according to the manufacturer's protocol. Briefly, the ice cold 10x PBS and 1 N NaOH were mixed and COL stock was added while kept on ice. The cell pellet was resuspended and mixed into the non-gelated COL mixture followed by immediate gelation in RT and the cell culture medium was added on top of the gelated hydrogels.

2.2 Mechanical testing

The acellular GG-SPD, GG-BaG, and COL hydrogel samples were mechanically tested by compression testing. The 0.875 cm^3 samples (n=3–6) of approximately 4.0–6.5 mm of height and 12.2 mm diameter were cast in custom-made molds and incubated overnight at +37°C under parafilm without media to ensure complete hydrogel gelation before compression testing or media incubation initiation. Unconfined compression was performed with a constant 10 mm/min strain rate in air environment in RT to 65 % strain from their original height at 0, 14, and 21 days of incubation in OM or BaG OM media. The compressive load was measured by the Bose 5100 BioDynamic ElectroForce (TA Instruments, New Castle, DE, USA) instrument equipped with a 225 N load sensor and the data was recorded with the WinTest 4.1 software (WinTest, Yokohama, Japan). The compressive modulus under tension was calculated by MS Excel (Microsoft, Redmond, WA, USA) based on the slope of the linear region of the stress versus strain curve where the Hooke's law holds [17].

2.3 Adipose stem cell isolation and cell expansion

The hASCs were obtained from subcutaneous adipose tissue of six healthy female donors of 52±5 years in surgeries at the Tampere University Hospital Department of Plastic Surgery between 2014–2015 with the patients' written informed consent, in accordance with the Ethics Committee of the Pirkanmaa Hospital District's, Tampere, Finland, ethical approval (R15161). The hASCs were isolated as reported previously [22]. Briefly, the adipose tissue was cut up and tissue was digested by collagenase type I (1.5 mg/mL; Thermo Fisher Scientific) in maintenance medium containing DMEM/F-12 1:1 (Thermo Fisher Scientific), 5 % human serum (Biowest, Nuaillé, France), 1 % L-glutamine (GlutaMAX; Thermo Fisher Scientific), and 1 % P/S. The cells were expanded in maintenance medium . Flow cytometry analysis was performed, and the overall results of the cell surface marker flow cytometry analysis (see Supplementary file 1) indicated the mesenchymal

origin of the cells in accordance with literature [3, 23, 24]. The isolated hASCs were tested and reported negative for mycoplasma contamination.

2.4 Osteogenic induction and cell culture

Osteogenic induction was initiated immediately after plating by adding 0.3 cm^3 either OM optimized for hASC osteogenic differentiation [22] or BaG OM to the hydrogel encapsulated cell constructs. The cells were plated at a density of 950,000 cells/cm^3, encapsulated in respective hydrogels which were cast in 48-well plate wells (Nunclon; Sigma-Aldrich) in a volume of 0.2 cm^3. The BaG ext was prepared as reported previously from bioactive glass 2-06 (wt-%: Na_2O 12.1; K_2O 14.0; CaO 19.8; P_2O_5 2.5; B_2O_3 1.6; SiO_2 50.0) [13]. Briefly, 87.5 mg/mL of BaG granules (500–1000 µm) of bioactive glass 2-06 were disinfected with 70 % ethanol washes for 10 min repeated twice and air dried in RT for 2 h followed by incubation for 24 h at +37°C to dissolve ions into the maintenance medium without human serum. After incubation, 5 % human serum (Biowest) was added to the sterile filtered (0.2 µm) BaG ext. The BaG ext was prepared fresh each 14 days to avoid any risk of precipitates. For the Raman spectroscopy analyses, the cells were cultured in phenol red free media to avoid fluorescence interference with the Raman spectra [13]. The control cell cultures were maintained in OM. Different media compositions are listed in Table 1. During the experiments, medium was changed every other day. The experiments were carried out at hASC passage 3–6.

Table 1. Composition of media.

Medium	Composition
Maintenance medium (MM)	DMEM/F-12 1:1, 5 % HS, 1 % L-glutamine, 1 % P/S
Osteogenic medium (OM)	5 nM Dex, 250 μM AsA2P, 10 mM β-GP in MM
BaG osteogenic medium (BaG OM)	OM in BaG ext base
Raman spectroscopy cell culture medium	Phenol red free DMEM/F-12 1:1 including L-glutamine, 5 % HS, 1 % P/S
Raman spectroscopy phenol red free BaG OM	OM in phenol red free BaG ext base

MM, maintenance medium; OM, osteogenic medium; BaG OM, bioactive glass extract osteogenic medium; HS, human serum (Biowest); P/S, 100 U/mL penicillin/streptomycin (Lonza); Dex, dexamethasone (Sigma-Aldrich); AsA2P, L-ascorbic acid 2-phosphate (Sigma-Aldrich); β-GP, beta-glycerophosphate (Sigma-Aldrich); L-glutamine (Thermo Fisher Scientific).

2.5 Cell viability and cell number

Cell viability was analyzed with Live/Dead fluorescence staining (Thermo Fisher Scientific) at 3 and 14 days, as described previously [25]. The living cells were stained with 0.5 mM calcein acetoxymethyl ester (green stain) and necrotic cells were stained with 0.25 mM ethidium homodimer-1 (red stain) for 45 min in RT. The samples were imaged using an epifluorescence Olympus IX51 microscope and Olympus DP30BW digital camera (Olympus, Tokyo, Japan).

Cell number was measured based on the total amount of DNA with CyQUANT Cell Proliferation Assay Kit (Thermo Fisher Scientific) according to the manufacturer's protocol at 14 and 21 days. Briefly, the cells were lysed with 0.1 % Triton X-100 buffer (Sigma-Aldrich) and the hydrogel samples were homogenized mechanically by the Ultra-Turrax tissue homogenizer (IKA Labortechnik, Staufen, Germany). The lysed samples were stored at –80°C until analysis after a freeze-thaw cycle. A working solution was prepared with the kit provided CyQUANT GR dye and

Cell lysis buffer. Fluorescence of 3 parallel samples was measured at 480/520 nm with Victor 1420 Multilabel Counter microplate reader (PerkinElmer, Waltham, MA, USA).

2.6 Immunocytochemical analysis

For the immunocytochemical analysis, the hydrogel samples with encapsulated cells were fixed with 4 % paraformaldehyde (PFA; Sigma-Aldrich). The cells were permeabilized with 0.1 % Triton X-100 buffer (Sigma-Aldrich) in blocking solution of 10 % normal donkey serum (Sigma-Aldrich) and 1 % bovine serum albumin (Sigma-Aldrich) for 1 h in RT. After washes with solution of 0.1 % Triton X-100 buffer, 1 % normal donkey serum , and 1 % bovine serum albumin , the hydrogel embedded cells were incubated with a mouse monoclonal anti-osteocalcin antibody (OCG3; dilution 1:100) detecting human osteocalcin (OC; Abcam, Cambridge, United Kingdom) for 72 h at +4°C [17]. Highly cross-adsorbed donkey anti-mouse IgG Alexa Fluor 488 secondary antibody (dilution 1:400; Thermo Fisher Scientific) was used for overnight staining at +4°C, and the cell nuclei were stained with 4’,6-diamidino-2-phenylindole (DAPI; dilution 1:2000; Sigma-Aldrich). The samples were imaged using an epifluorescence Olympus IX51 microscope and Olympus DP30BW digital camera (Olympus). OC stained in cyan-green was imaged at 488 nm and cell nuclei stained in blue color by DAPI were detected at 361 nm.

2.7 Mineralization

For the hASC mineralization assay, the hASC secreted hydroxyapatite residues of the cell matrix in 3D hydrogel were stained with the OsteoImage assay according to manufacturer’s protocol (OsteoImage Mineralization Assay; Lonza) at 21 days [26]. Briefly, the cells were fixed with 4 % PFA (Sigma-Aldrich) for 30 min in RT and the hydroxyapatite residues were stained with the OsteoImage Staining Reagent for 45 min and immediately measured at 490/535 nm with Victor 1420 Multilabel Counter microplate reader (PerkinElmer). After quantitative measurement, the cell nuclei were stained with DAPI (dilution 1:2000) and detected at 361 nm together with the stained

hydroxyapatite residues imaged at 492/520 nm with an epifluorescence Olympus IX51 microscope and Olympus DP30BW digital camera (Olympus).

2.8 Quantitative real-time polymerase chain reaction

Quantitative real-time polymerase chain reaction (qRT-PCR) method was applied to analyze the relative expression of osteogenic marker genes. Total sample RNA from 2 parallel samples was isolated at 7 and 14 days with the NucleoSpin RNA II kit (Macherey-Nagel, Düren, Germany) according to the kit protocol. High-Capacity cDNA Reverse Transcriptase Kit (Applied Biosystems, Foster City, CA, USA) was used to synthesize first strand complementary DNA (cDNA) of the total RNA. The gene expression of human intestinal *alkaline phosphatase* (*ALPL*), *runt related transcription factor 2* (*RUNX2*), *distal-less homeobox 5* (*DLX5*), and *osterix* (*OSX*) was measured. A mathematical data analysis model was applied to calculate the relative gene expression of each sample in relation to a housekeeping gene human *ribosomal protein lateral stalk subunit P0* (*RPLP0*) [27]. The measured gene expression data was normalized to that of *RPLP0* [28, 29]. The mixture for qRT-PCR analysis consisted of 50 ng cDNA, 300 nM forward and reverse primers, and SYBR Green PCR Master Mix (Applied Biosystems). The primer sequences and accession numbers are listed in Table 2. All primers were purchased from Oligomer (Helsinki, Finland). The ABI PRISM 7300 Sequence Detection System (Applied Biosystems) was used for the qRT-PCR initial reactions at +95°C for 10 min enzyme activation, and followed by 45 cycles at +95°C for 15 s denaturation, and 60 s annealing and extension at +60°C.

Table 2. The primer sequences for qRT-PCR.

Name	Primer	5'-Sequence-3'	Product size (bp)	Accession number
RPLP0	Fwd	AATCTCCAGGGGCACCATT	70	NM_001002
	Rev	CGCTGGCTCCCACTTTGT		
ALPL	Fwd	CCCCCGTGGCAACTCTATCT	73	NM_000478.5
	Rev	GATGGCAGTGAAGGGCTTCTT		
RUNX2	Fwd	CTTCATTCGCCTCACAAACAAC	62	NM_001024630.3
	Rev	TCCTCCTGGAGAAAGTTTGCA		
DLX5	Fwd	ACCATCCGTCTCAGGAATCG	75	NM_005221.5
	Rev	CCCCCGTAGGGCTGTAGTAGT		
OSX	Fwd	TGAGCTGGAGCGTCATGTG	79	NM_152860.1
	Rev	TCGGGTAAAGCGCTTGGA		

2.9 Optical Projection Tomography and Selective Plane Illumination Microscopy

In-house-built SPIM and OPT multimodal 3D imaging systems were used to image hASCs encapsulated in the transparent GG-SPD hydrogels [20, 21], whereas the opacity of the COL hydrogel prevented its imaging. The structure and distribution of the hASCs and their ECM in the 3D hydrogel was obtained with the brightfield OPT, and 3D fluorescence signal of the OsteoImage (Lonza) stained hydroxyapatite residues was captured with the SPIM. The hydrogel-cell samples cultured initially in 1.0-cm inside diameter fluorinated ethylene propylene (FEP; Adtech Polymer Engineering, Stroud, United Kingdom) tubes were punctured with 1.0-mm inside diameter FEP tubes to insert the cell-laden hydrogels into the smaller tubes for imaging. For the brightfield OPT imaging of the samples, a white light LED source (LTCL23; Opto Engineering, Mantova, Italy) was used to illuminate the sample in transmission mode without any contrasting agents. A total of 400 projection images were captured with 0.9°-degree intervals using a 20x water-immersed objective while rotating the sample 360° degrees. The 3D images of hASCs and ECM were reconstructed using filtered back projection algorithm (Matlab; MathWorks, Natick, MA, USA) [19]. The brightfield OPT imaged a smaller cylindrical volume (d=0.67 mm, h=0.67 mm) within a larger cylindrical volume (d=1 mm, h= sample height) inside the spatial area of the 1.0-mm diameter FEP

tube whereas the fluorescence SPIM imaged a larger rectangular volume (x=0.67 mm, y=0.67 mm, z=1 mm) due to differences in technical imaging modalities.

For the SPIM fluorescence imaging, the cell-laden GG hydrogels inside the 1.0-cm inside diameter FEP tube were fixed with 4 % PFA (Sigma-Aldrich) for 1 h and the hydroxyapatite residues were stained for 90 min in RT to allow stain diffusion throughout the hydrogel volume (OsteoImage Mineralization Assay, Lonza). The SPIM illumination light sheet at 488 nm wavelength (Custom multi-wavelength laser system, Modulight, Tampere, Finland) was used to excite sample fluorescence. In the detection path, notch filter (NF03-405/488/561/635E-25 StopLine Quad-Notch filter; Semrock, Rochester, NY, USA) was used to cut out the excitation light from the fluorescent signal emitted by mineralized residues. The fluorescence image stack was acquired by translating the sample in the axial direction of the detection path and capturing an image every 3 µm with a x20 objective. The image stack was acquired in z direction while x and y directions formed the actual image. Both OPT and SPIM images were visualized in 3D using Avizo 9.3 (FEI Visualization Sciences Group; Thermo Fisher Scientific).

2.10 Raman spectroscopy

The inorganic phosphate PO_4^{3-} containing hydroxyapatite mineral residues of the hASC-secreted cell matrix in different hydrogels were analyzed semi-quantitatively by Raman spectroscopic methods [30]. In the preliminary experiments, we verified that the Raman spectra of the mineralized hASC matrix in 3D hydrogels in the BaG OM condition and that of added pure hydroxyapatite powder (0.5 or 2.5 mg/mL) acellular hydrogels were identical in terms of observed Raman shift at 960 cm^{-1} (see Supplementary file 2). For the Raman experiments, hASCs from 1 donor, and GG-SPD, GG-BaG, and COL cell-laden and parallel cell-free samples in a phenol red free BaG OM condition were analyzed at 21 days avoiding interference of phenol red fluorescence to Raman spectra. The OM condition was omitted from analysis due to COL hydrogel contraction and the low detection of the GG-SPD mineralized matrix in OM. The Raman spectroscopy was conducted as

described in [30] and prior to analysis, the cell-hydrogel samples were washed with 1x PBS. Briefly, the Raman scattering was generated with a fiber coupled pulsed laser (532 nm, 150 ps, 40–100 kHz) (TimeGate Instruments, Oulu, Finland). The spectra were collected from a single location by averaging Raman signal from 2.1 million laser pulses produced in 47 s. The reference spectra of cell-free samples measured in identical conditions were subtracted from the measured data. The obtained spectra for each sample were normalized to average intensity between 475–560 cm^{-1}.

2.11 Statistical methods

The significance of differences between mean ranks for equal distributions was determined using Mann-Whitney U Test for statistical significance with *p*-values < 0.05. For the mechanical testing results, 3–6 parallel samples were tested in each experiment group (n=3–6). The cell number analyses were repeated with 3 different hASC donors with 3 parallel samples for each condition (n=9). The gene expression analyses were repeated for 3 different donors with 2 parallel samples for each condition (n=6). The mineralization assay was conducted with hASCs from 3 donors with 1–2 parallel samples for the GG-SPD in OM and BaG OM groups (n=5), whereas for COL in BaG OM, hASCs from only 2 donors were tested with 2 parallel samples (n=4) due to contracted gels. All the COL in OM hydrogel mineralization samples were contracted after 3 days of culture, and therefore, unavailable for mineralization quantification analysis at 21 days. The data was analyzed with IBM SPSS Statistics 23 software (IBM, Armonk, NY, USA).

3. Results

3.1 Mechanical properties of hydrogels improved by serum-containing media incubation

The acellular GG-SPD and COL hydrogel samples in OM and BaG OM media, and GG-BaG in OM alone, were mechanically tested by compression testing at 0, 14, and 21 days of incubation (Fig. 1).

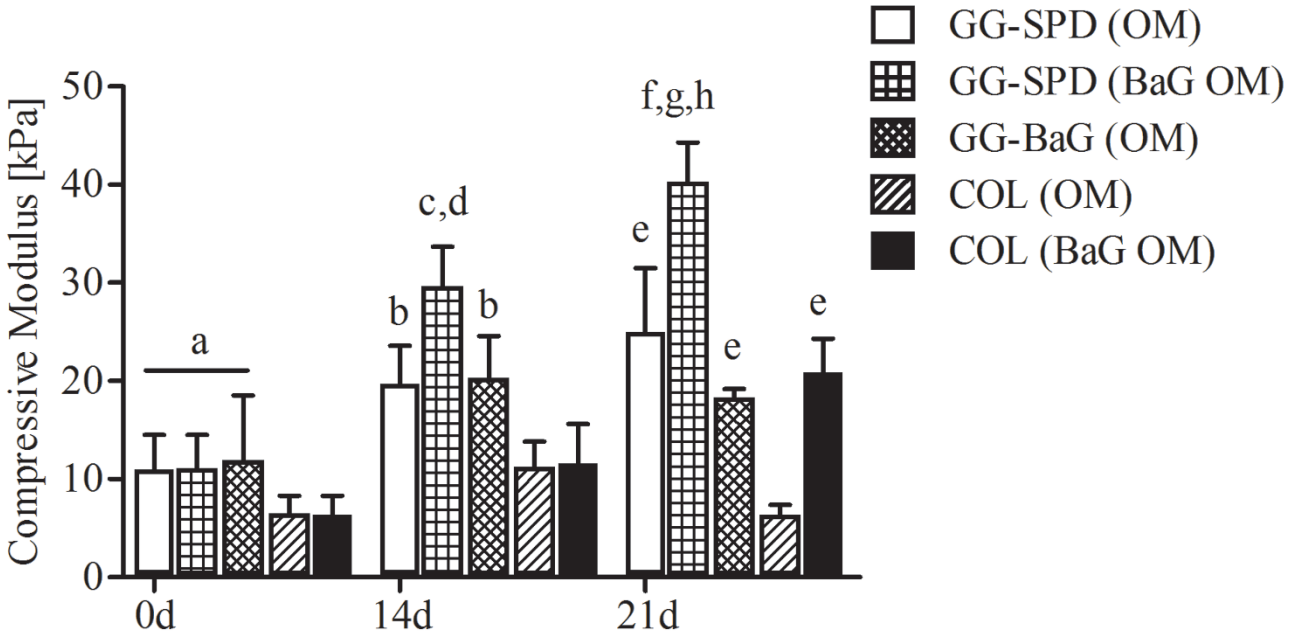

Fig. 1 Compressive moduli. Cell-free GG-SPD, GG-BaG, and COL hydrogels after 0-day, 14-day, and 21-day incubation in OM and BaG OM media, where GG-BaG in OM only (n=3–6). Data are presented as mean + SD. Significant difference with $p < 0.05$. **a** Significant difference from COL hydrogel samples at 0 days; **b** Significant difference from COL (OM) at 14 days; **c** Significant difference from GG-SPD (OM) at 14 days; **d** Significant difference from GG-BaG (OM) at 14 days; **e** Significant difference from COL (OM) at 21 days; **f** Significant difference from GG-SPD (OM) at 21 days; **g** Significant difference from GG-BaG (OM) at 21 days; **h** Significant difference from COL (BaG OM) at 21 days. *1-column fitting figure.*

The measured compressive moduli of acellular GG-SPD hydrogels with both the OM and BaG OM incubation and those of GG-BaG with the OM incubation increased, indicating additional ionic crosslinking. At day 0, the compressive moduli of all the GG samples without medium incubation were statistically significantly higher than those for the COL hydrogel samples. The OM condition increased the moduli of all hydrogels in the beginning, however, only GG-SPD moduli continued to increase in OM after the 14-day time point. Furthermore, the modulus of GG-SPD was significantly higher than that of GG-BaG in OM although the modulus of GG-BaG with the OM incubation was significantly higher compared to COL in OM at both 14- and 21-day time points. Indeed, the BaG

OM incubation alone increased COL compressive modulus significantly at 21 days. Additionally, at 21 days, the GG-SPD (BaG OM) samples had the highest compressive moduli measured at approximately 40.0 kPa and significantly higher compared to GG-SPD (OM) and COL (BaG OM). For both GG-SPD and COL hydrogels, the BaG OM condition had significantly higher compressive modulus compared to the OM condition at the 21-day time point. Overall, the COL as well as GG-BaG samples showed ductile behavior and plastic deformation properties without a fracture point, whereas by default, the GG-SPD samples had higher resistance to deformation and more brittle behavior which indicated a stiffer structure, and also had a clear fracture point in the stress-strain curve (See Supplementary file 3).

3.2 Adipose stem cell viability maintained and cell number increased in 3D hydrogels

The viability of hASCs was analyzed at 3 and 14 days of 3D hydrogel culture (Fig. 2, see Supplementary file 4). The cells remained well viable during culture. The COL (OM) samples contracted after 4 days and were therefore unavailable for a later time point.

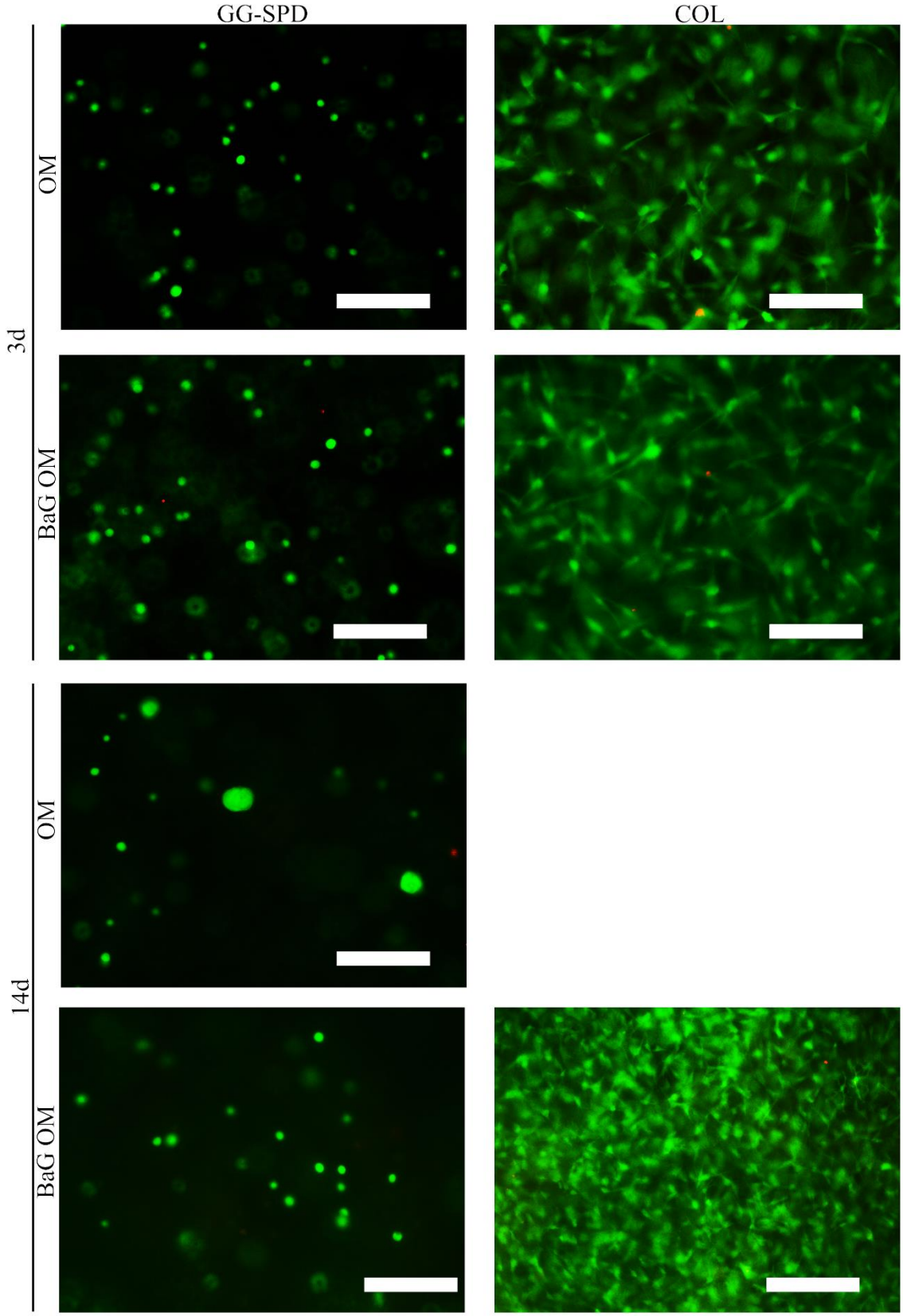

Fig. 2 Cell viability. Viability of hASCs encapsulated in GG-SPD (OM), GG-SPD (BaG OM), COL (OM) and COL (BaG OM) 3D hydrogels at 3 and 14 days. The COL (OM) samples

contracted after 3 days. Representative images with hASCs from 1 donor (*n*=1). Scale bar 200 µm. *Figure in color in print. 2-column fitting figure.*

The cell number based on total DNA content was analyzed at 14- and 21-day time points (Fig. 3).

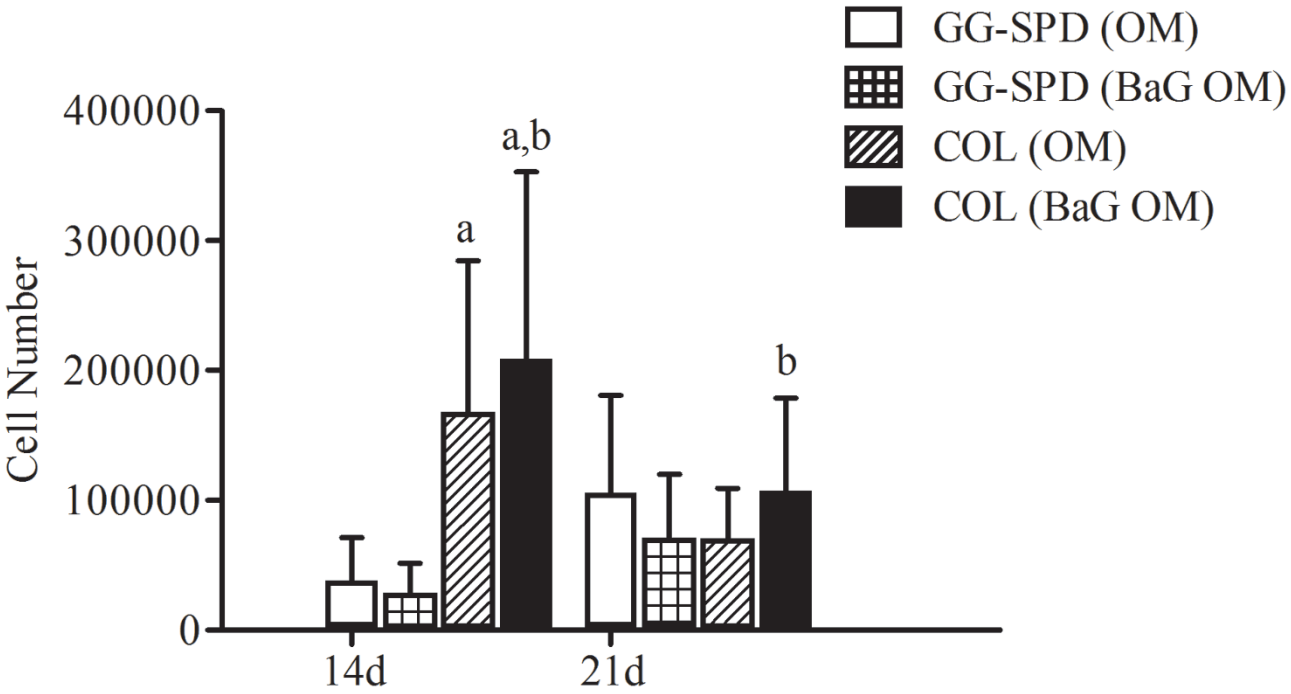

Fig. 3 Cell number. Cell number based on total DNA content of hASCs encapsulated in 3D hydrogels at 14 and 21 days. The analyzed hASCs were from 3 donors (*n*=9). Data are presented as mean + SD. Significant difference with $p < 0.05$. **a** The combined COL (OM) and COL (BaG OM) cell numbers are significantly higher compared to the combined GG-SPD (OM) and GG-SPD (BaG OM) cell numbers at 14 days; **b** The combined 14- and 21-day COL (BaG OM) cell numbers are significantly higher compared to the combined 14- and 21-day GG-SPD (BaG OM) cell numbers. *1-column fitting figure.*

The cell number increased the most for the BaG OM cultured samples with the significantly highest cell number for the COL (BaG OM) at 14 days. Also, at 14 days, the COL hydrogels in OM and BaG OM combined together had a significantly higher cell number compared to the combined GG-SPD hydrogels in OM and BaG OM. Further, the combined cell number results at 14 and 21 days of

the COL (BaG OM) condition showed a significantly higher cell number compared to the combined 14- and 21-day GG-SPD (BaG OM) cell numbers.

3.3 Higher expression of osteogenic marker genes of adipose stem cells in collagen type I hydrogel scaffolds

The gene expression of osteogenic marker genes was analyzed by qRT-PCR at 14 and 21 days (Fig. 4).

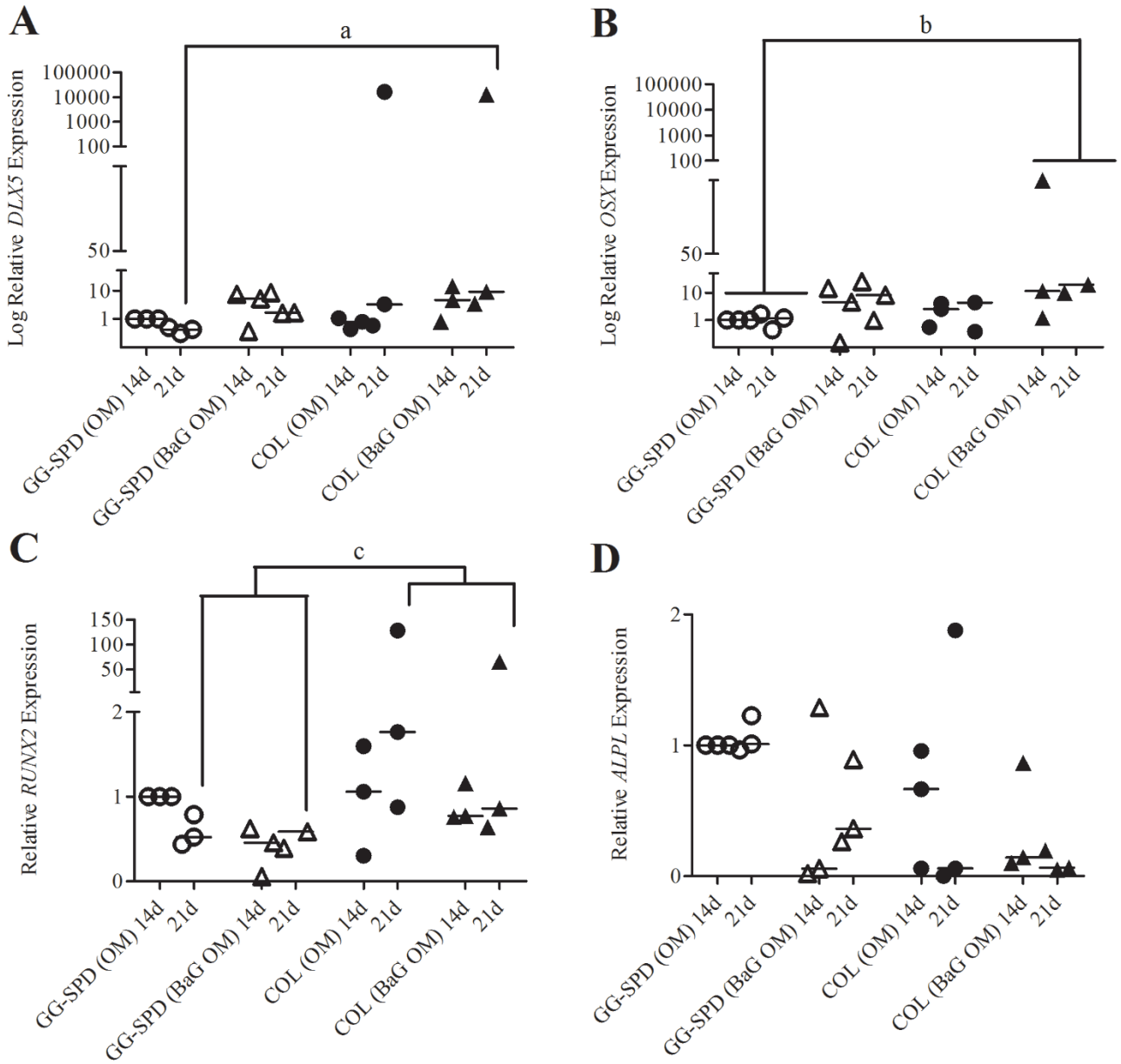

Fig. 4 Gene expression. Gene expression of osteogenic marker genes of hASCs in GG-SPD (OM), GG-SPD (BaG OM), COL (OM), and COL (BaG OM) 3D hydrogels at 14 and 21 days. Significant difference with $p < 0.05$. (**A**) *DLX5* gene expression significantly higher in **a** COL (BaG OM) compared to GG-SPD (OM) at 21 days; (**B**) *OSX* gene expression significantly higher for **b** the combined COL (OM) and COL (BaG OM) sample expression at 14 and 21 days compared to the combined GG-SPD (OM) and GG-SPD (BaG OM) sample expression at 14 and 21 days; (**C**) *RUNX2* gene expression significantly higher for **c** the combined COL (OM) and COL (BaG OM) sample expression at 21 days compared to the combined GG-SPD (OM) and GG-SPD (BaG OM) sample expression at 21 days; (**D**) *ALPL* gene expression. The results were relativised to the control condition of GG-SPD (OM) at 14 days. The relative expression of *DLX5* and *OSX* had high variance and are presented partly in Log(10) scale. The hASCs were isolated from 3 donors (n=6). Group medians are indicated with a horizontal line. *1.5-column fitting figure.*

All the osteogenic marker genes were statistically significantly higher in gene expression in COL in OM or in BaG OM compared to GG-SPD at 3 weeks, excluding *ALPL* expression. Due to the non-Gaussian distribution, the statistical analyses of the gene expression medians was conducted with the Mann-Whitney test. The *DLX5* expression was significantly higher for the COL (BaG OM) compared to GG-SPD (OM) at 21 days. The *OSX* expression was significantly higher for the combined COL (BaG OM) results at 14 and 21 days compared to the combined results for GG-SPD (OM) at 14 and 21 days. The gene expression of *RUNX2* of the combined COL in OM and BaG OM samples at 21 days was statistically significantly higher than that of the combined GG-SPD samples in OM and BaG OM at the 21-day time point.

3.4 Strong immunocytochemical osteocalcin staining of adipose stem cells in collagen type I hydrogel scaffolds

Immunocytochemical staining results of OC and DAPI stained hASCs encapsulated in GG and COL hydrogels in different media conditions at 21 days are shown in Fig. 5 (see Supplementary file 5).

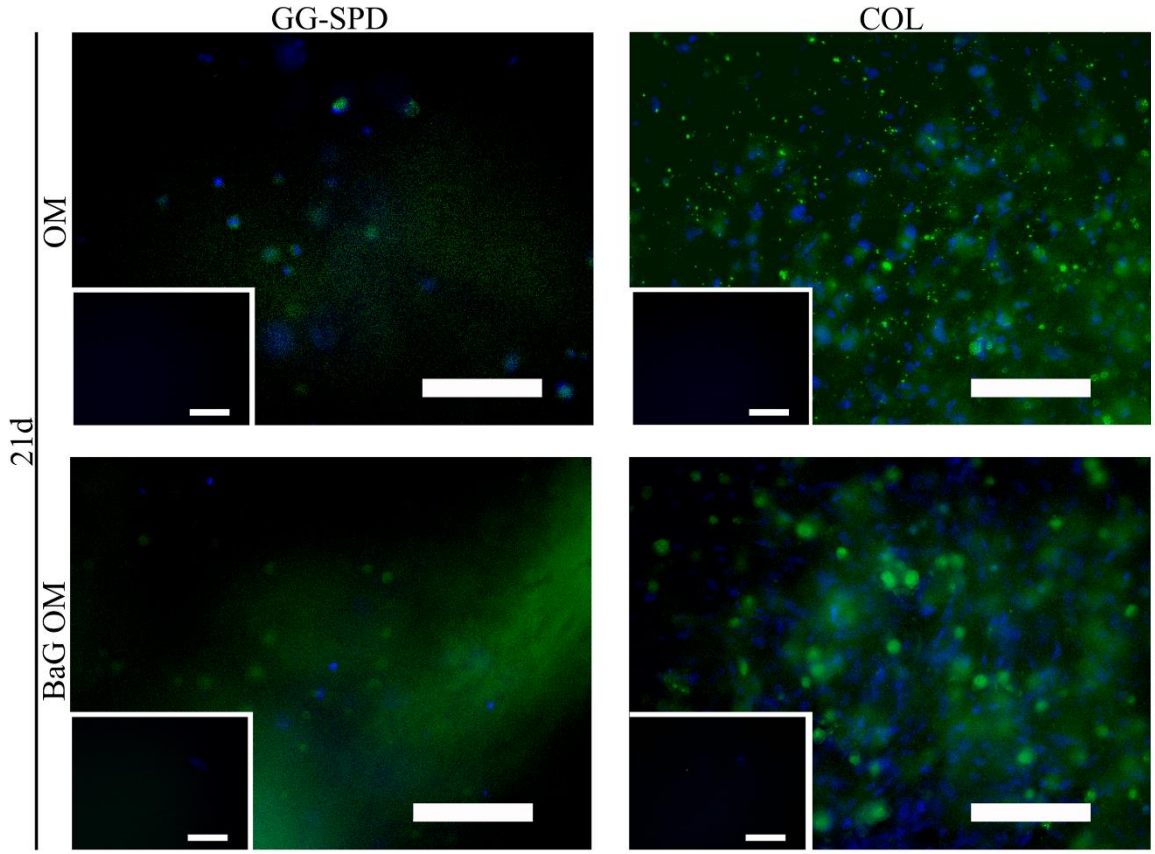

Fig. 5 Osteocalcin immunofluorescence staining. Representative images of osteocalcin and DAPI stained hASCs in GG-SPD (OM), GG-SPD (BaG OM), COL (OM), and COL (BaG OM) 3D hydrogels at 21 days. The blank controls are shown in lower left corner. The hASCs were isolated from 2 donors (n=2). Scale bar 200 µm. *Figure in color in print. 2-column fitting figure.*

Strong OC immunofluorescence staining was detected in the COL samples in both media conditions, although some OC staining in GG-SPD was visible.

3.5 Efficient mineralization of adipose stem cells in 3D hydrogel scaffolds

The hASC secreted mineralized matrix of hydroxyapatite residues were stained with the OsteoImage assay and hASC nuclei with DAPI and imaged in 3D hydrogels at 21 days (Fig. 6A). The hydroxyapatite content was also quantified with the OsteoImage assay analysis (Fig. 6B).

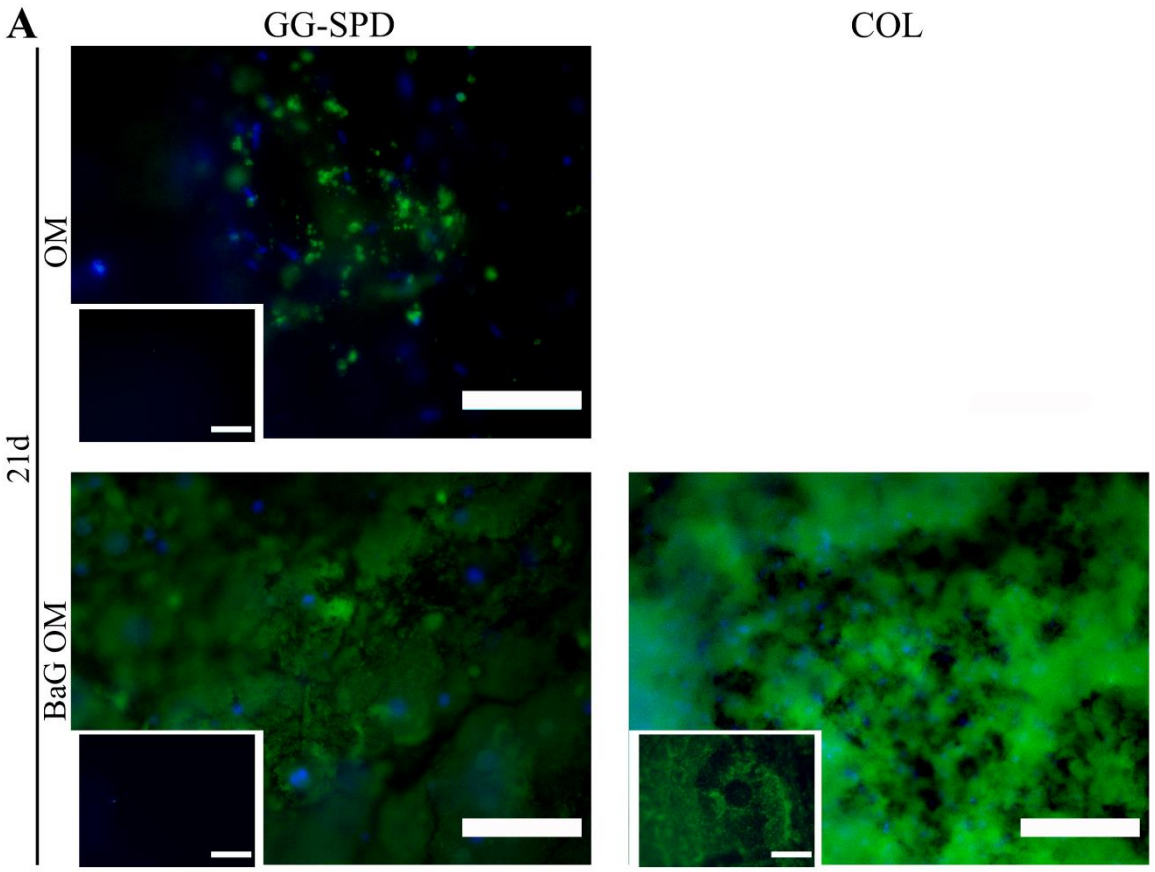

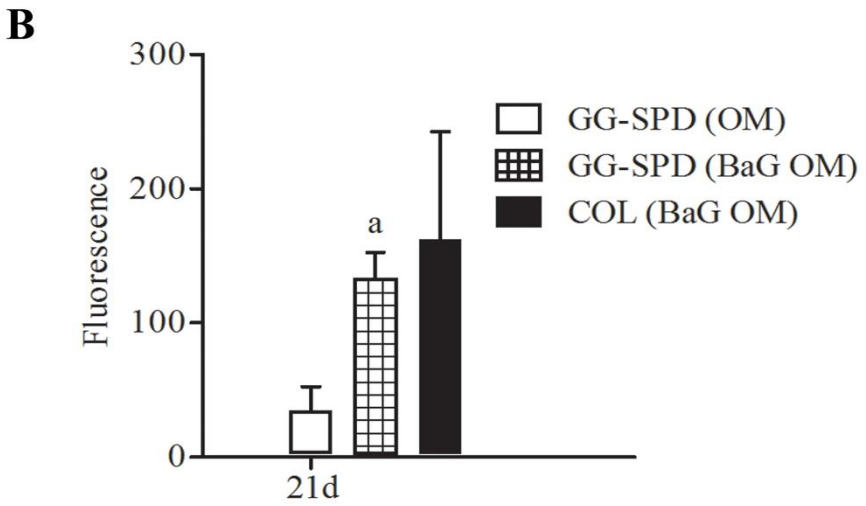

Fig. 6 Mineralization. (**A**) Representative images of hydroxyapatite residues and cell nuclei of hASCs stained with the OsteoImage assay and DAPI in 3D hydrogels at 21 days in GG-SPD (OM), GG-SPD (BaG OM), and COL (BaG OM). The COL (OM) samples contracted before 21 days. The blank controls are presented in the lower left corner. The hASCs were isolated from 1 donor (n=1). Scale bar 200 µm; (**B**) The measured OsteoImage hydroxyapatite mineralization fluorescence count of hASCs in 3D hydrogel at 21 days. Data are presented as mean + SD. **a** Significant difference from GG-SPD (OM) with $p < 0.05$. The hASCs were isolated from 3 donors and 2 parallel samples of each condition were tested, out of which for GG-SPD (OM) and (BaG OM) groups a total of 5 samples (n=5), and for COL (BaG OM) 4 samples (n=4) were available for analysis at 21-day time point. *Figure in color in print. 2-column fitting figure.*

The OsteoImage stained hydroxyapatite residue imaging supported the quantified mineralization results with the strongest hydroxyapatite staining for the COL (BaG OM), while also strong staining was seen in the GG-SPD (BaG OM) condition, and where moderate staining was visible in the GG-SPD (OM) at the 21-day time point.

3.6 Optical Projection Tomography and Selective Plane Illumination Microscopy for high resolution 3D hydrogel scaffold imaging

OPT and SPIM images were acquired for brightfield transmission and fluorescence emission modes, respectively (Fig. 7). Optical opacity of the COL hydrogel prevented its OPT and SPIM imaging.

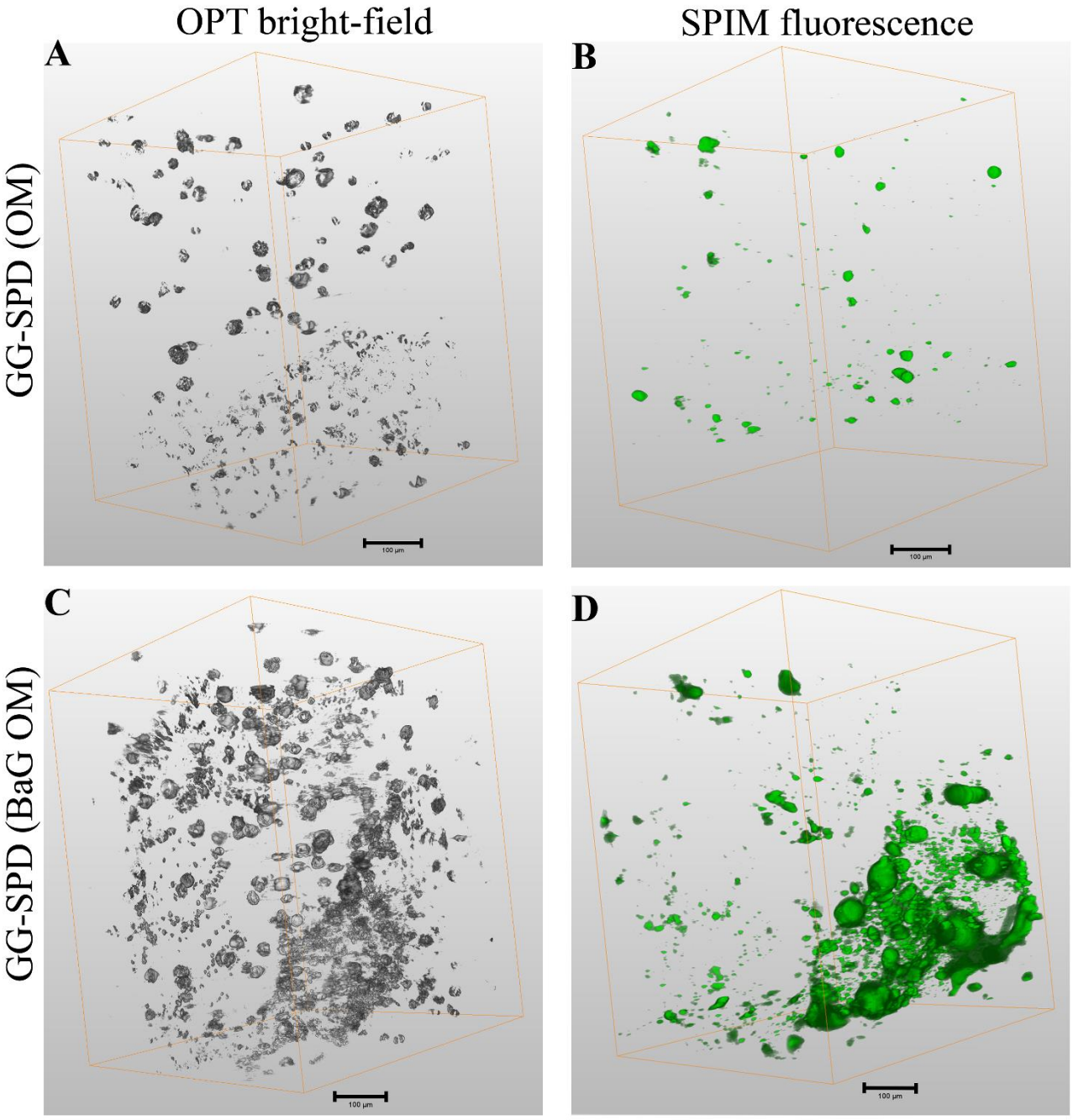

Fig. 7 OPT and SPIM 3D imaging of hASC-hydrogel constructs. Representative label-free brightfield OPT 3D reconstructed images of hASCs encapsulated in (**A**) GG-SPD (OM); (**C**) GG-SPD (BaG OM); and OsteoImage hydroxyapatite stained fluorescence SPIM 3D images of hASCs in 3D hydrogels in (**B**) GG-SPD (OM); (**D**) GG-SPD (BaG OM) at 21 days. The hASCs were isolated from 1 donor (*n*=1). Scale bar 100 µm. *Figure in color in print. 2-column fitting figure.*

For the brightfield OPT 3D reconstructed images, the variation in light attenuation between the cells and the hydrogel structure allowed to visualize the distribution of the cells in each projection image (Fig. 7A; 7C; see Supplementary file 9; 10; 3D reconstruction videos). The cells and the surrounding shaded mineralized ECM were visible in transmission mode brightfield images, and thus offered proof of concept that label-free OPT can be applied to 3D hydrogel cell culture mineralization studies. The 3D stack of multi-focal fluorescence SPIM imaging showed the fluorescent-labeled mineralization clearly with strong hydroxyapatite stain in the GG-SPD (BaG OM) sample (Fig. 7B; 7D; see Supplementary file 11; 12; 3D reconstruction videos) whereas the fluorescent-stained hydroxyapatite was scarce in the OM condition (see Supplementary file 13; 14; 3D reconstruction video). Any closer inspection of cell morphology was restricted by the optically dense mineralization.

3.7 Raman spectroscopic analysis verified mineralized hydroxyapatite residues and gellan gum mineralization improved with bioactive glass extract ionic crosslinking

The Raman spectra of hASCs in GG-SPD (BaG OM), GG-BaG (BaG OM) and COL (BaG OM) were measured at 21 days (Fig. 8).

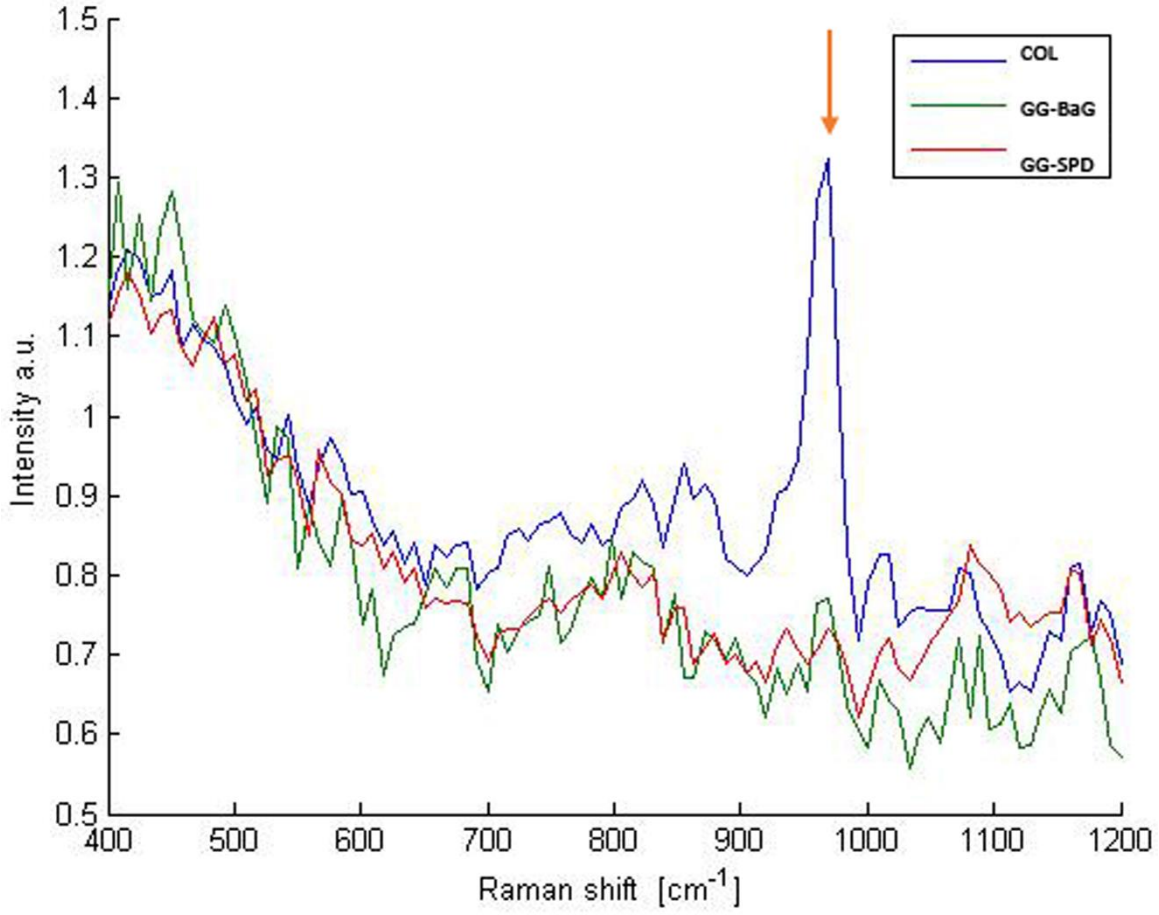

Fig. 8 Raman spectroscopic analysis. The hASC secreted mineralized residue Raman shifts in 3D hydrogel at 21 days in GG-SPD (BaG OM) (red), GG-BaG (BaG OM) (green) and COL (BaG OM) (blue) conditions. The red arrow points to the phosphate peak at Raman shift 960 cm^{-1}. The hASCs were isolated from 1 donor (*n*=1). The spectra were normalized to average intensity between 475–560 cm^{-1}. *Figure in color in print. 1.5-column fitting figure.*

The measured Raman spectra showed the detected phosphate peak at Raman shift 960 cm^{-1} indicating semi-quantitatively hydroxyapatite residue content for all the measured samples with the highest result for the COL (BaG OM) sample which confirmed the quantified OsteoImage mineralization as well as the imaged hydroxyapatite staining results (Fig. 6). Additionally, Fig. 9 presents measured fluorescence of the hydroxyapatite residues in GG-SPD (OM) and GG-BaG (OM) samples at 3 weeks (see Supplementary file 6 for crosslinker comparison results on cell

viability; Supplementary file 7 for crosslinker comparison cell number results; Supplementary file 8 for crosslinker comparison hydroxyapatite mineralization imaging results).

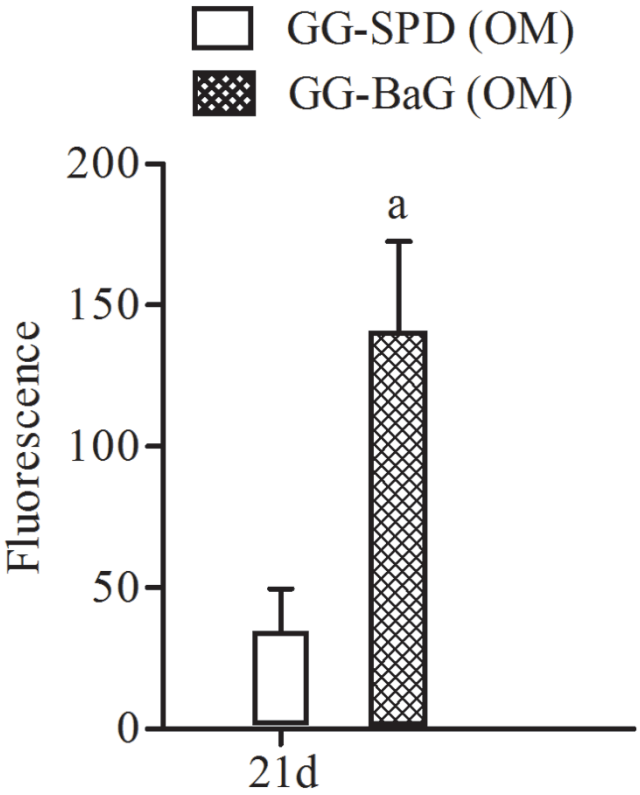

Fig. 9 Mineralization with different gellan gum crosslinkers. The measured fluorescence count for the OsteoImage stained hydroxyapatite mineralization of hASCs in GG-SPD and GG-BaG hydrogel samples in OM at 21 days. The analyzed hASCs were from 3 donors (n=9). Data are presented as mean + SD. **a** Significant difference from GG-SPD (OM) with p = 0.002. *1-column fitting figure.*

The slightly higher semi-quantitative phosphate peak detected at Raman shift 960 cm^{-1} for the GG-BaG (BaG OM) (Fig. 8) followed a similar trend to the measured significantly higher hydroxyapatite content for the GG-BaG (OM) compared to GG-SPD (OM) at 3 weeks (Fig. 9).

4. Discussion

Presently, efficient bone grafts are urgently called for, and in order to help answer this demand, we studied a novel bone tissue engineering approach with BaG OM induction of hASCs embedded in

GG and COL 3D hydrogels. The BaG OM induction of hASCs has been found promising for bone applications and to support rapid hASC osteogenic differentiation already in our previous work [13]. In the present study, we hypothesized that the BaG OM could induce hASCs osteogenesis in 3D when embedded into GG and COL hydrogels together with gradually evolving hydrogel mechanical properties, and thus yield a sufficiently stiff, while also flexible and osteoinductive matrix mimicking bone organic and inorganic phase composite structure [31, 32] for the development of engineered bone constructs. Also, injectable hydrogels are especially attractive biomaterials due to their malleability as bone defects are typically of varied dimensions [15]. To ensure hydrogel construct suitability for bone applications, the mechanical properties of GG-SPD, GG-BaG, and COL hydrogels were analyzed with compression testing. Our results for non-incubated GG and COL hydrogel moduli were supported by previous reports [33, 34]. The softer COL and GG-BaG hydrogel scaffolds followed a similar trend in the OM with a seeming improvement of mechanical properties up to 14 days, and then degrading at 21 days. Interestingly, the GG-BaG hydrogel resulted in a weaker gel compared to the GG-SPD in OM, albeit the GG-BaG hydrogels were stable and showed sufficient mechanical properties and a modulus comparable to COL hydrogel in BaG OM at 3 weeks. The relatively weak mechanical properties of GG and the lack of COL stability have limited their potential for hard tissue applications [6, 16]. However, we demonstrated significantly improved mechanical properties for both GG-SPD and COL hydrogels with the BaG OM incubation. Indeed, the GG-SPD (BaG OM) samples had the highest compressive modulus measured at 40 kPa, and therefore, potential for bone-like graft development when compared to the approximated 30 kPa modulus required for an osteoblastic matrix [4, 35-37]. Even though these mechanical properties would be sufficient in small bone cavities to support the development of an osteoblastic matrix, in load-bearing bone defects a scaffold for additional stabilization would be required. Significantly, also COL hydrogel mechanical properties were gradually reinforced with the BaG OM incubation. Although a similar strengthening by added

BaG particles in GG and COL hydrogels has been reported [4, 16], we significantly improved hydrogel scaffold mechanical properties with ionic BaG dissolution products alone. Importantly, the gradual hydrogel stiffening in BaG OM incubation might mimic the evolving bone matrix mechanical properties of natural bone formation process [31, 36-38].

We tested 3D hydrogel culture cytocompatibility, and the hydrogel encapsulated hASCs were mostly alive at 14 days, as expected since the GG-SPD cell-hydrogel constructs have shown previously good cytocompatibility in 3D culture with human pluripotent stem cell-derived neuronal cells [17]. Moreover, the observed rounded morphology of hASCs embedded in GG-SPD in both OM and BaG OM was expected and suggested lack of adhesion sites, since GG hydrogel encapsulated human cells have been found to require functionalization also in other studies [17, 39]. Interestingly, rounded cell morphology could be irrelevant regarding hASC capacity for osteogenic differentiation encapsulated in GG [6, 37]. Conversely, in COL efficient cell adhesion was seen not only in the spreading of the hASCs embedded in COL hydrogel, but also in the strong tendency of the cells to pull on the matrix and make the COL samples contract in the OM condition. This issue has been reported in various studies [7, 16, 33, 40], however, importantly for novelty, we showed that the BaG OM incubation significantly improved the COL mechanical stability and rendered the COL hydrogel scaffolds more resistant to cell-induced contraction. We also detected a decrease in the cell number from 14 to 21 days in the COL hydrogels in parallel with enhanced osteogenic differentiation, similarly to a previously reported 2D study in our group [13], whereas there was a small albeit nonsignificant increase in cell number in the GG-SPD hydrogels between day 14 and 21.

According to our initial hypothesis of strong osteogenic induction of hASCs with BaG ionic species, we saw that the hASC osteogenic marker gene expression results of *DLX5* and *OSX* were significantly higher in COL (BaG OM) hydrogels, although the gene expression medians were also elevated in the GG-SPD (BaG OM) condition. This showed the effect of the BaG OM incubation

with additional synergistic support of the 3D COL hydrogel matrix for hASC osteogenesis. Similarly to the current results, the bioactive glass 2-06 based BaG OM has been previously reported to increase hASC gene expression of *RUNX2* [13]. Moreover, the gene expression of *RUNX2* was more strongly enhanced in the control condition of OM for COL hydrogel samples which attested further of the COL 3D hydrogel support for efficient hASC osteogenic differentiation.Instead, no visible trend was discernible in gene expression of early bone marker *ALPL*, however, the bioactive glass 2-06 based BaG OM has been shown to promote efficacious hASC mineralization despite low alkaline phosphatase activity [13]. Indeed, low gene expression of *ALPL* might be due to the more advanced state of mineralization. Also, the mineralization results attested of robust hASC osteogenesis with the strong hydroxyapatite residue accumulation in the hASC-secreted matrix with BaG OM in both the GG and COL hydrogels. Importantly, the clear peak of inorganic phosphate containing hydroxyapatite mineral residues visible in the Raman spectra attested of considerable mineralized cell matrix accumulation. The Raman spectroscopic results verified the hASC osteogenic activity and hydroxyapatite accumulation in the cell-secreted mineralized ECM, also seen in the OsteoImage mineralization results. Furthermore, the semi-quantitative Raman spectra attested similar succession of samples as the mineralization assay in the BaG OM condition, where COL had the highest hydroxyapatite content, followed by GG-BaG and the lesser amount detected for hASCs in the GG-SPD hydrogel samples. However, the non-homogenous character of the cell-secreted mineralized matrix might have interfered with the semi-quantitative Raman measurement results. The 3D reconstructed OPT and stacked fluorescence SPIM images showed homogeneously deposited hydroxyapatite surrounding or in close proximity to hydrogel encapsulated hASCs approximating ECM growth. The cell distribution was similar by visual inspection in both conditions as seen in the brightfield OPT 3D reconstructed images, however, the fluorescence SPIM images showed a stronger mineral deposition of the hASC secreted matrix in the BaG OM condition compared to OM. These 3D reconstructed images supported

further the measured OsteoImage results where hydroxyapatite fluorescence count was significantly higher for the hASC-laden GG-SPD (BaG OM) samples compared to OM at 3 weeks. Our results demonstrated the attractiveness and efficacy of high resolution OPT and SPIM imaging techniques for 3D mesoscopic imaging of transparent wet-state cell-laden hydrogel samples with a refractive index close to water providing a real 3D image of the sample while avoiding issues of photobleaching or low spatial resolution of conventional fluorescence microscopy. While OPT has been applied for high resolution (< 1 μm) imaging of optically transparent small animal embryos in developmental biology [41-44], our in-house built OPT system has also been employed to assess hydrogel macrostructure [19] as well as 3D cell cultures [21]. Additionally, brightfield OPT allowed to inspect the general aspect of the mineral depositions together with the cells, however, the signal was label-free and therefore non-specific. Nonetheless, the brightfield OPT imaging showed potential for a label-free mineralization imaging technique for future studies. What is more, these techniques permitted the 3D imaging of cells in an unaltered hydrogel microstructure in a wet-state. Importantly, the SPIM and also the label-free OPT imaging allowed to study the cell and mineralized matrix distribution spanning the whole 3D volume and thus avoiding the mere surface effect of hydrogel mineralization where an apatite layer has been deposited on top of the incubated hydrogel samples [45]. Indeed, the BaG ability to cause hydroxyapatite precipitation in 3D hydrogel culture with embedded cells in the presence of biological fluid has been reported also in other studies [4, 5, 15, 46-48]. However, previously only moderate hydroxyapatite staining of human mesenchymal stem cells with osteogenic induction has been shown in 3D hydrogel culture [26] compared to our robust results. Similarly to a prior study by Gantar et al., we achieved hydroxyapatite deposition in hASC-secreted ECM in central parts of GG-SPD hydrogel samples, whereas in contrast, we used BaG OM ionic dissolution products alone without embedded BaG nanoparticles [4]. Although the cell-free COL samples showed some background as expected, due to the fact that COL functions as a natural platform for mineral crystal accumulation in acellular

mineralization processes [5, 7], the mineral deposition was clearly accelerated in interactions with the cell-secreted matrix in our present results. Moreover, these results verified that the GG-SPD hydrogels allowed the steady unobstructed diffusion [20] of the ionic species supporting hASC osteogenic differentiation and homogeneous mineral deposition. What is more, the cell-containing samples were also positively stained for the late osteogenic marker OC, which was shown to increase together with the quantitatively measured and imaged mineralized content thus confirming hASC osteogenic differentiation towards bone-like cells in 3D hydrogel culture. All in all, the strong OC and hydroxyapatite staining in the COL hydrogel, in addition to the highest Raman spectroscopic measurement result indicated that COL hydrogel combined with the BaG OM as the most efficient osteogenic inducer of the hydrogel encapsulated hASCs. In the future and especially for *in vivo* studies for larger critical sized bone defects, however, cell survival, diffusion of nutrients, and removal of waste products also in the central parts of the construct should be secured with an adequate vessel structure for vascularized bone-like graft development. Also, the effect of mineralization on collagen hydrogel *in vivo* degradation would require further investigation in the future.

While COL hydrogel has been extensively tested for potential injectable bone tissue engineering applications [5, 49-51], we also tested an abundant and economic GG hydrogel for hASC osteogenic differentiation. On the whole, our results indicated that the BaG OM induction was required for efficient hASC osteogenic differentiation encapsulated in 3D GG-SPD and COL hydrogels. The BaG OM was chosen based on previous studies in our group that showed in 2D culture the efficiency of the bioactive glass 2-06 BaG ext for hASC osteogenic induction [13]. Importantly, the current results confirmed that the dissolved BaG ions with the OM supplements together with evolving hydrogel mechanical properties were efficient to induce hASC osteogenic differentiation. Further, we hypothesized that crosslinking GG hydrogel with the BaG ext would enhance hASC mineralization encapsulated in 3D GG, based on the rich Ca^{2+} content of the BaG

ext and since GG crosslinking requires small cations [52]. Also, Ca^{2+} ions are implicated in the ECM mineralization process [46]. Indeed, the poor performance of cell-loaded GG hydrogel samples in control OM was rescued by Ca^{2+} crosslinking with the BaG ext. What is more, the mineralization results suggested that a separate cationic crosslinker might be omitted when using the novel BaG ext for GG gelation, where a statistically significantly higher hydroxyapatite content of the hASC-laden GG-BaG hydrogels was compared to GG-SPD samples in control OM at 3 weeks. Further studies are still required to determine the potential of the BaG ext hydrogel crosslinking for the hASC mineralization process in more detail.

Overall, BaG OM induced efficient osteogenic differentiation and strong mineralization of hASCs in 3D hydrogels thus supporting further the osteoblast-like cell maturation combined with enhanced mechanical properties of the mineralized matrix in both the GG and COL hydrogels. Therefore, these novel results combining osteoinducing BaG ions and 3D hydrogel stem cell culture have considerable potential for the development of a wide variety of applications for bone tissue engineered constructs.

5. Conclusions

In this study, we studied enhanced hASC osteogenic induction with BaG ionic dissolution products in GG-SPD and COL 3D hydrogel culture in BaG OM compared to regular OM. Incubation in BaG OM significantly reinforced GG and COL hydrogel mechanical properties and showed a stiffening behavior similar to an evolving bone matrix. In both media conditions, the hASCs were well viable embedded within 3D hydrogel, where the GG-SPD encapsulated hASCs had a tight and round cell morphology, whereas in COL hydrogel elongated and spread morphologies were observed. With the BaG OM induction, the hASCs in COL hydrogel showed significantly higher osteogenic marker gene expression. On the whole, the BaG OM culture significantly enhanced hASC potency to mineralize in both the GG-SPD and COL 3D hydrogels, however, hASC-laden COL (BaG OM) hydrogels showed highest mineralization and hydroxyapatite content confirmed by Raman

spectroscopy analysis together with the strongest OC staining results. Importantly, the BaG ext-crosslinked GG-BaG hydrogels promoted significantly higher hASC mineralization even in the control OM. The OPT and SPIM techniques were evaluated as efficient methods for emerging 3D hydrogel cell culture imaging and analysis applications. These results demonstrated the significant potential of BaG OM induction and novel 3D hydrogel culture methods for the osteogenic differentiation of hASCs towards bone-like cells and for bone regeneration applications.

Competing interests

The authors declare that they have no competing interests.

Funding

This study was financially supported by the Finnish Funding Agency for Innovation (TEKES Business Finland), the Human Spare Parts Project, the Academy of Finland, The City of Tampere Science Fund, The Finnish Cultural Foundation's Pirkanmaa Regional Fund, The Finnish Foundation for Technology Promotion, and the Competitive State Research Financing of the Expert Responsibility area of Tampere University Hospital.

Authors' contributions

KV contributed to planning of the work, carried out most of the data collection and analysis, drafted and edited the manuscript. MO contributed to planning of the work and participated in manuscript preparation and editing. JK, HHä, BB, and TM participated in data collection and analysis and manuscript preparation and editing. HHu was consulted for statistical analyses, contributed to the data analysis and participated in manuscript preparation and editing. LH, MK, JH, and JI participated in the planning of the work and manuscript preparation and editing. SM contributed to planning and coordination of the work, interpretation of data, and participated in manuscript preparation and editing.

Acknowledgements

The authors wish to thank Mari Lehti-Polojärvi, MSc, for the OPT and SPIM imaging cell culture platforms, Computational Biophysics and Imaging Group, BioMediTech, Faculty of Medicine and Health Technology, Tampere University, Tampere, Finland, , the Tampere Imaging Facility (TIF), Tampere University, for their support in imaging services, and Jenny Parraga Meneses, PhD, Biomaterials and Tissue Engineering Group, BioMediTech, Faculty of Medicine and Health Technology, Tampere University, Finland , and Nick Walters, PhD, Adult Stem Cell Group, BioMediTech, Faculty of Medicine and Health Technology, Tampere University, Tampere, Finland , and for technical support Adult Stem Cell Group laboratory technicians Miia Juntunen, MSc, Anna-Maija Honkala, laboratory engineer, and Sari Kalliokoski.

Supplementary material

Supplementary file 1: Flow cytometric analysis and cell characterization.docx. Flow cytometric surface marker expression analysis and cell characterization results.

Supplementary file 2: Raman spectra of acellular hydrogels.docx. Raman spectra of acellular blank and acellular hydroxyapatite doped hydrogel constructs.

Supplementary file 3: Representative stress-strain curves.docx. Compressive modulus mechanical testing of cell-free GG-SPD, GG-BaG, and COL hydrogels after 0-, 14-, and 21-day incubation in OM and BaG OM media.

Supplementary file 4: Cell viability.docx. Viability of hASCs encapsulated in GG-SPD (OM), GG-SPD (BaG OM), COL (OM) and COL (BaG OM) 3D hydrogels at 3 and 14 days.

Supplementary file 5: Immunocytochemical staining of osteocalcin.docx. Osteocalcin production and nuclei of hASCs encapsulated in GG-SPD (OM), GG-SPD (BaG OM), COL (OM) and COL (BaG OM) 3D hydrogels at 21 days.

Supplementary file 6: Cell viability crosslinker comparison.docx. Viability of hASCs encapsulated in GG-SPD (OM) and GG-BaG (OM) 3D hydrogels at 3, 14, and 21 days.

Supplementary file 7: Cell number crosslinker comparison.docx. Cell number based on total DNA content of hASCs encapsulated in GG-SPD (OM) and GG-BaG (OM) 3D hydrogels at 14 and 21 days.

Supplementary file 8: Mineralization crosslinker comparison.docx. OsteoImage hydroxyapatite and DAPI staining of hASCs encapsulated in GG-SPD (OM) and GG-BaG (OM) 3D hydrogels at 21 days.

Supplementary file 9: Brightfield OPT imaging of GG-SPD in OM.avi. Brightfield OPT imaging 3D reconstruction of GG-SPD cell-hydrogel construct in OM condition at 21 days.

Supplementary file 10: Brightfield OPT imaging of GG-SPD in BaG OM.avi. Brightfield OPT imaging 3D reconstruction of GG-SPD cell-hydrogel construct in BaG OM condition at 21 days.

Supplementary file 11: Fluorescence SPIM imaging of GG-SPD in BaG OM.avi. Fluorescence SPIM imaging 3D reconstruction of GG-SPD cell-hydrogel construct with fluorescence stained hydroxyapatite in BaG OM condition at 21 days.

Supplementary file 12: Combined OPT and SPIM imaging of GG-SPD in BaG OM.avi. Combined OPT and SPIM imaging 3D reconstruction of GG-SPD cell-hydrogel construct in BaG OM condition at 21 days.

Supplementary file 13: Fluorescence SPIM imaging of GG-SPD in OM.avi. Fluorescence SPIM imaging 3D reconstruction of GG-SPD cell-hydrogel construct with fluorescence stained hydroxyapatite in OM condition at 21 days.

Supplementary file 14: Combined OPT and SPIM imaging of GG-SPD in OM.avi. Combined OPT and SPIM imaging 3D reconstruction of GG-SPD cell-hydrogel construct in OM condition at 21 days.

Vitae

Kaisa Vuornos, MSc, works as a doctoral student in the Adult Stem Cell Group, BioMediTech, Faculty of Medicine and Health Technology, Tampere University, Tampere, Finland.

Miina Ojansivu, PhD, works as a post doctoral researcher at the Karolinska Institutet, Solna, Sweden, in the Department of Medical Biochemistry and Biophysics.

Janne T Koivisto, MSc, works as a doctoral student in the Biomaterials and Tissue Engineering Group, BioMediTech, Faculty of Medicine and Health Technology, Tampere University, Tampere, Finland, and also works in the Heart Group, BioMediTech, Faculty of Medicine and Health Technology, Tampere University, Tampere, Finland.

Heikki Häkkänen works as a Laboratory Engineer in the Spectroscopy for Detecting Dynamics of Biomolecules Group, Nanoscience Center, in the Department of Biological and Environmental Science in the University of Jyväskylä, Jyväskylä, Finland.

Birhanu Belay, MSc, works as a doctoral student in the Computational Biophysics and Imaging Group, BioMediTech, at the Faculty of Medicine and Health Technology, Tampere University, Tampere, Finland.

Toni Montonen, MSc, works as a doctoral student in the Computational Biophysics and Imaging Group, BioMediTech, at the Faculty of Medicine and Health Technology, Tampere University, Tampere, Finland.

Heini Huhtala, MSc, works as a University Instructor in the Faculty of Social Sciences, Tampere University, Tampere, Finland.

Minna Kääriäinen, MD, PhD, works as a plastic surgeon and chief physician in the Department of Plastic and Reconstructive Surgery at the Tampere University Hospital, Tampere, Finland.

Leena Hupa, DSc, is the Professor of Inorganic Chemistry at the Johan Gadolin Process Chemistry Centre, Åbo Akademi University, Åbo, Finland.

Professor Minna Kellomäki, DSc, is the Principal Investigator of the Biomaterials and Tissue Engineering Group, BioMediTech, Faculty of Medicine and Health Technology, Tampere University, Finland.

Professor Jari Hyttinen, DSc, is the Principal Investigator in the Computational Biophysics and Imaging Group (www.tut.fi/cbig), BioMediTech, at the Faculty of Medicine and Health Technology, Tampere University, Tampere, Finland.

Professor Janne A Ihalainen, PhD, is the Principal Investigator in the Spectroscopy for Detecting Dynamics of Biomolecules Group, Nanoscience Center, and the Head of Department in the Department of Biological and Environmental Science in the University of Jyväskylä, Jyväskylä, Finland.

Susanna Miettinen, PhD, is an Associate Professor in the Faculty of Medicine and Health Technology in the Tampere University and the Principal Investigator in the Adult Stem Cell Group, BioMediTech, Faculty of Medicine and Health Technology, Tampere University, Tampere, Finland.

References

[1] A. Chatterjea, G. Meijer, C. van Blitterswijk, J. de Boer, Clinical application of human mesenchymal stromal cells for bone tissue engineering, Stem Cells Int., (2010) 215625. 10.4061/2010/215625 [doi].

[2] M. Jakob, F. Saxer, C. Scotti, S. Schreiner, P. Studer, A. Scherberich, M. Heberer, I. Martin, Perspective on the evolution of cell-based bone tissue engineering strategies, Eur.Surg.Res., 49 No. 1 (2012) 1-7. 10.1159/000338362 [doi].

[3] B. Lindroos, R. Suuronen, S. Miettinen, The potential of adipose stem cells in regenerative medicine, Stem Cell.Rev., 7 No. 2 (2011) 269-291. 10.1007/s12015-010-9193-7 [doi].

[4] A. Gantar, L.P. da Silva, J.M. Oliveira, A.P. Marques, V.M. Correlo, S. Novak, R.L. Reis, Nanoparticulate bioactive-glass-reinforced gellan-gum hydrogels for bone-tissue engineering, Mater.Sci.Eng.C.Mater.Biol.Appl., 43 (2014) 27-36. 10.1016/j.msec.2014.06.045 [doi].

[5] A.K. Miri, N. Muja, N.O. Kamranpour, W.C. Lepry, A.R. Boccaccini, S.A. Clarke, S.N. Nazhat, Ectopic bone formation in rapidly fabricated acellular injectable dense collagen-Bioglass hybrid scaffolds via gel aspiration-ejection, Biomaterials, 85 (2016) 128-141. 10.1016/j.biomaterials.2016.01.047 [doi].

[6] M.B. Oliveira, C.A. Custodio, L. Gasperini, R.L. Reis, J.F. Mano, Autonomous osteogenic differentiation of hASCs encapsulated in methacrylated gellan-gum hydrogels, Acta Biomater., 41 (2016) 119-132. 10.1016/j.actbio.2016.05.033 [doi].

[7] B. Marelli, C.E. Ghezzi, D. Mohn, W.J. Stark, J.E. Barralet, A.R. Boccaccini, S.N. Nazhat, Accelerated mineralization of dense collagen-nano bioactive glass hybrid gels increases scaffold stiffness and regulates osteoblastic function, Biomaterials, 32 No. 34 (2011) 8915-8926. 10.1016/j.biomaterials.2011.08.016 [doi].

[8] T.E.L. Douglas, A. Lapa, S.K. Samal, H.A. Declercq, D. Schaubroeck, A.C. Mendes, P.V. der Voort, A. Dokupil, A. Plis, K. De Schamphelaere, I.S. Chronakis, E. Pamula, A.G. Skirtach, Enzymatic, urease-mediated mineralization of gellan gum hydrogel with calcium carbonate, magnesium-enriched calcium carbonate and magnesium carbonate for bone regeneration applications, J.Tissue Eng.Regen.Med., 11 No. 12 (2017) 3556-3566. 10.1002/term.2273 [doi].

[9] M.G. Manda, L.P. da Silva, M.T. Cerqueira, D.R. Pereira, M.B. Oliveira, J.F. Mano, A.P. Marques, J.M. Oliveira, V.M. Correlo, R.L. Reis, Gellan gum-hydroxyapatite composite spongy-

like hydrogels for bone tissue engineering, J.Biomed.Mater.Res.A., 106 No. 2 (2018) 479-490. 10.1002/jbm.a.36248 [doi].

[10] L.L. Hench, Biomaterials: a forecast for the future, Biomaterials, 19 No. 16 (1998) 1419-1423. S0142-9612(98)00133-1 [pii].

[11] L.L. Hench, The future of bioactive ceramics, J.Mater.Sci.Mater.Med., 26 No. 2 (2015) 86-015-5425-3. Epub 2015 Feb 3. 10.1007/s10856-015-5425-3 [doi].

[12] L.L. Hench & J. Wilson, Biocompatibility of silicates for medical use, Ciba Found.Symp., 121 (1986) 231-246.

[13] M. Ojansivu, S. Vanhatupa, L. Bjorkvik, H. Hakkanen, M. Kellomaki, R. Autio, J.A. Ihalainen, L. Hupa, S. Miettinen, Bioactive glass ions as strong enhancers of osteogenic differentiation in human adipose stem cells, Acta Biomater., 21 (2015) 190-203. 10.1016/j.actbio.2015.04.017 [doi].

[14] M. Ojansivu, L. Hyvari, M. Kellomaki, L. Hupa, S. Vanhatupa, S. Miettinen, Bioactive glass induced osteogenic differentiation of human adipose stem cells is dependent on cell attachment mechanism and mitogen-activated protein kinases, Eur.Cell.Mater., 35 (2018) 54-72. 10.22203/eCM.v035a05 [doi].

[15] T.E. Douglas, W. Piwowarczyk, E. Pamula, J. Liskova, D. Schaubroeck, S.C. Leeuwenburgh, G. Brackman, L. Balcaen, R. Detsch, H. Declercq, K. Cholewa-Kowalska, A. Dokupil, V.M. Cuijpers, F. Vanhaecke, R. Cornelissen, T. Coenye, A.R. Boccaccini, P. Dubruel, Injectable self-gelling composites for bone tissue engineering based on gellan gum hydrogel enriched with different bioglasses, Biomed.Mater., 9 No. 4 (2014) 045014-6041/9/4/045014. Epub 2014 Jul 25. 10.1088/1748-6041/9/4/045014 [doi].

[16] A. El-Fiqi, J.H. Lee, E.J. Lee, H.W. Kim, Collagen hydrogels incorporated with surface-aminated mesoporous nanobioactive glass: Improvement of physicochemical stability and

mechanical properties is effective for hard tissue engineering, Acta Biomater., 9 No. 12 (2013) 9508-9521. 10.1016/j.actbio.2013.07.036 [doi].

[17] J.T. Koivisto, T. Joki, J.E. Parraga, R. Paakkonen, L. Yla-Outinen, L. Salonen, I. Jonkkari, M. Peltola, T.O. Ihalainen, S. Narkilahti, M. Kellomaki, Bioamine-crosslinked gellan gum hydrogel for neural tissue engineering, Biomed.Mater., 12 No. 2 (2017) 025014-605X/aa62b0. 10.1088/1748-605X/aa62b0 [doi].

[18] R. Lopez-Cebral, P. Paolicelli, V. Romero-Caamano, B. Seijo, M.A. Casadei, A. Sanchez, Spermidine-cross-linked hydrogels as novel potential platforms for pharmaceutical applications, J.Pharm.Sci., 102 No. 8 (2013) 2632-2643. 10.1002/jps.23631 [doi].

[19] E. Figueiras, A.M. Soto, D. Jesus, M. Lehti, J. Koivisto, J.E. Parraga, J. Silva-Correia, J.M. Oliveira, R.L. Reis, M. Kellomaki, J. Hyttinen, Optical projection tomography as a tool for 3D imaging of hydrogels, Biomed.Opt.Express, 5 No. 10 (2014) 3443-3449. 10.1364/BOE.5.003443 [doi].

[20] A.M. Soto, J.T. Koivisto, J.E. Parraga, J. Silva-Correia, J.M. Oliveira, R.L. Reis, M. Kellomaki, J. Hyttinen, E. Figueiras, Optical Projection Tomography Technique for Image Texture and Mass Transport Studies in Hydrogels Based on Gellan Gum, Langmuir, 32 No. 20 (2016) 5173-5182. 10.1021/acs.langmuir.6b00554 [doi].

[21] B. Belay, J.T. Koivisto, K. Vuornos, T. Montonen, O. Koskela, M. Lehti-Polojärvi, S. Miettinen, M. Kellomäki, E. Figueiras, J. Hyttinen, Optical Projection Tomography Imaging of Single Cells in 3D Gellan Gum Hydrogel, (2017), IFMBE Proceedings EMBEC & NBC 2017, Springer Nature Singapore Pte Ltd. 2018, Singapore.

[22] L. Kyllonen, S. Haimi, B. Mannerstrom, H. Huhtala, K.M. Rajala, H. Skottman, G.K. Sandor, S. Miettinen, Effects of different serum conditions on osteogenic differentiation of human adipose stem cells in vitro, Stem Cell.Res.Ther., 4 No. 1 (2013) 17. 10.1186/scrt165.

[23] M. Dominici, K. Le Blanc, I. Mueller, I. Slaper-Cortenbach, F. Marini, D. Krause, R. Deans, A. Keating, D. Prockop, E. Horwitz, Minimal criteria for defining multipotent mesenchymal stromal cells. The International Society for Cellular Therapy position statement, Cytotherapy, 8 No. 4 (2006) 315-317. 10.1080/14653240600855905.

[24] K. McIntosh, S. Zvonic, S. Garrett, J.B. Mitchell, Z.E. Floyd, L. Hammill, A. Kloster, Y. Di Halvorsen, J.P. Ting, R.W. Storms, B. Goh, G. Kilroy, X. Wu, J.M. Gimble, The immunogenicity of human adipose-derived cells: temporal changes in vitro, Stem Cells, 24 No. 5 (2006) 1246-1253. 2005-0235 [pii].

[25] L. Tirkkonen, S. Haimi, S. Huttunen, J. Wolff, E. Pirhonen, G.K. Sandor, S. Miettinen, Osteogenic medium is superior to growth factors in differentiation of human adipose stem cells towards bone-forming cells in 3D culture, Eur.Cell.Mater., 25 (2013) 144-158.

[26] L.A. Castillo Diaz, M. Elsawy, A. Saiani, J.E. Gough, A.F. Miller, Osteogenic differentiation of human mesenchymal stem cells promotes mineralization within a biodegradable peptide hydrogel, J.Tissue Eng., 7 (2016) 2041731416649789. 10.1177/2041731416649789 [doi].

[27] M.W. Pfaffl, A new mathematical model for relative quantification in real-time RT-PCR, Nucleic Acids Res., 29 No. 9 (2001) e45.

[28] T. Fink, P. Lund, L. Pilgaard, J.G. Rasmussen, M. Duroux, V. Zachar, Instability of standard PCR reference genes in adipose-derived stem cells during propagation, differentiation and hypoxic exposure, BMC Mol.Biol., 9 (2008) 98-2199-9-98. 10.1186/1471-2199-9-98 [doi].

[29] B.G. Gabrielsson, L.E. Olofsson, A. Sjogren, M. Jernas, A. Elander, M. Lonn, M. Rudemo, L.M. Carlsson, Evaluation of reference genes for studies of gene expression in human adipose tissue, Obes.Res., 13 No. 4 (2005) 649-652. 10.1038/oby.2005.72 [doi].

[30] P. Ruokola, E. Dadu, A. Kazmertsuk, H. Hakkanen, V. Marjomaki, J.A. Ihalainen, Raman spectroscopic signatures of echovirus 1 uncoating, J.Virol., 88 No. 15 (2014) 8504-8513. 10.1128/JVI.03398-13 [doi].

[31] W.L. Murphy, T.C. McDevitt, A.J. Engler, Materials as stem cell regulators, Nat.Mater., 13 No. 6 (2014) 547-557. 10.1038/nmat3937 [doi].

[32] N. Ramesh, S.C. Moratti, G.J. Dias, Hydroxyapatite-polymer biocomposites for bone regeneration: A review of current trends, J.Biomed.Mater.Res.B.Appl.Biomater., (2017) n. pag. 10.1002/jbm.b.33950 [doi].

[33] C.B. Raub, A.J. Putnam, B.J. Tromberg, S.C. George, Predicting bulk mechanical properties of cellularized collagen gels using multiphoton microscopy, Acta Biomater., 6 No. 12 (2010) 4657-4665. 10.1016/j.actbio.2010.07.004 [doi].

[34] J. Silva-Correia, A. Gloria, M.B. Oliveira, J.F. Mano, J.M. Oliveira, L. Ambrosio, R.L. Reis, Rheological and mechanical properties of acellular and cell-laden methacrylated gellan gum hydrogels, J.Biomed.Mater.Res.A., 101 No. 12 (2013) 3438-3446. 10.1002/jbm.a.34650 [doi].

[35] J.H. Wen, L.G. Vincent, A. Fuhrmann, Y.S. Choi, K.C. Hribar, H. Taylor-Weiner, S. Chen, A.J. Engler, Interplay of matrix stiffness and protein tethering in stem cell differentiation, Nat.Mater., 13 No. 10 (2014) 979-987. 10.1038/nmat4051 [doi].

[36] A.J. Engler, S. Sen, H.L. Sweeney, D.E. Discher, Matrix elasticity directs stem cell lineage specification, Cell, 126 No. 4 (2006) 677-689. S0092-8674(06)00961-5 [pii].

[37] N. Huebsch, P.R. Arany, A.S. Mao, D. Shvartsman, O.A. Ali, S.A. Bencherif, J. Rivera-Feliciano, D.J. Mooney, Harnessing traction-mediated manipulation of the cell/matrix interface to control stem-cell fate, Nat.Mater., 9 No. 6 (2010) 518-526. 10.1038/nmat2732 [doi].

[38] E.V. Alakpa, V. Jayawarna, A. Lampel, K.V. Burgess, C.C. West, S.C.J. Bakker, S. Roy, N. Javid, S. Fleming, D.A. Lamprou, J. Yang, A. Miller, A.J. Urquhart, P.W.J.M. Frederix, N.T. Hunt, B. Péault, R.V. Ulijn, M.J. Dalby, Tunable Supramolecular Hydrogels for Selection of Lineage-Guiding Metabolites in Stem Cell Cultures, Chem, 1 No. 2 (2016) 298-319. 10.1016/j.chempr.2016.07.001 [doi].

[39] J. Karvinen, J.T. Koivisto, I. Jonkkari, M. Kellomaki, The production of injectable hydrazone crosslinked gellan gum-hyaluronan-hydrogels with tunable mechanical and physical properties, J.Mech.Behav.Biomed.Mater., 71 (2017) 383-391. S1751-6161(17)30155-8 [pii].

[40] R.A. Perez, M. Kim, T.H. Kim, J.H. Kim, J.H. Lee, J.H. Park, J.C. Knowles, H.W. Kim, Utilizing core-shell fibrous collagen-alginate hydrogel cell delivery system for bone tissue engineering, Tissue Eng.Part A., 20 No. 1-2 (2014) 103-114. 10.1089/ten.TEA.2013.0198 [doi].

[41] J. Mayer, A. Robert-Moreno, R. Danuser, J.V. Stein, J. Sharpe, J. Swoger, OPTiSPIM: integrating optical projection tomography in light sheet microscopy extends specimen characterization to nonfluorescent contrasts, Opt.Lett., 39 No. 4 (2014) 1053-1056. 10.1364/OL.39.001053 [doi].

[42] J. Sharpe, Optical projection tomography, Annu.Rev.Biomed.Eng., 6 (2004) 209-228. 10.1146/annurev.bioeng.6.040803.140210 [doi].

[43] J. Sharpe, U. Ahlgren, P. Perry, B. Hill, A. Ross, J. Hecksher-Sorensen, R. Baldock, D. Davidson, Optical projection tomography as a tool for 3D microscopy and gene expression studies, Science, 296 No. 5567 (2002) 541-545. 10.1126/science.1068206 [doi].

[44] H.C. Chen, H.P. Lee, M.L. Sung, C.J. Liao, Y.C. Hu, A novel rotating-shaft bioreactor for two-phase cultivation of tissue-engineered cartilage, Biotechnol.Prog., 20 No. 6 (2004) 1802-1809. 10.1021/bp049740s [doi].

[45] J.A. Killion, S. Kehoe, L.M. Geever, D.M. Devine, E. Sheehan, D. Boyd, C.L. Higginbotham, Hydrogel/bioactive glass composites for bone regeneration applications: synthesis and characterisation, Mater.Sci.Eng.C.Mater.Biol.Appl., 33 No. 7 (2013) 4203-4212. 10.1016/j.msec.2013.06.013 [doi].

[46] H. Orimo, The mechanism of mineralization and the role of alkaline phosphatase in health and disease, J.Nippon Med.Sch., 77 No. 1 (2010) 4-12. JST.JSTAGE/jnms/77.4 [pii].

[47] A.J. Leite, B. Sarker, T. Zehnder, R. Silva, J.F. Mano, A.R. Boccaccini, Bioplotting of a bioactive alginate dialdehyde-gelatin composite hydrogel containing bioactive glass nanoparticles, Biofabrication, 8 No. 3 (2016) 035005-5090/8/3/035005. 10.1088/1758-5090/8/3/035005 [doi].

[48] J. Lewandowska-Lancucka, S. Fiejdasz, L. Rodzik, M. Koziel, M. Nowakowska, Bioactive hydrogel-nanosilica hybrid materials: a potential injectable scaffold for bone tissue engineering, Biomed.Mater., 10 No. 1 (2015) 015020-6041/10/1/015020. 10.1088/1748-6041/10/1/015020 [doi].

[49] B. Sarker, J. Hum, S.N. Nazhat, A.R. Boccaccini, Combining collagen and bioactive glasses for bone tissue engineering: a review, Adv.Healthc.Mater., 4 No. 2 (2015) 176-194. 10.1002/adhm.201400302 [doi].

[50] M.M. Villa, L. Wang, J. Huang, D.W. Rowe, M. Wei, Bone tissue engineering with a collagen-hydroxyapatite scaffold and culture expanded bone marrow stromal cells, J.Biomed.Mater.Res.B.Appl.Biomater., 103 No. 2 (2015) 243-253. 10.1002/jbm.b.33225 [doi].

[51] T. Long, J. Yang, S.S. Shi, Y.P. Guo, Q.F. Ke, Z.A. Zhu, Fabrication of three-dimensional porous scaffold based on collagen fiber and bioglass for bone tissue engineering, J.Biomed.Mater.Res.B.Appl.Biomater., 103 No. 7 (2015) 1455-1464. 10.1002/jbm.b.33328 [doi].

[52] E. Miyoshi, T. Takaya, K. Nishinari, Rheological and thermal studies of gel-sol transition in gellan gum aqueous solutions, Carbohydrate Polymers, 30 No. 2-3 (1996) 109-119.